Master's Thesis

Adhesion Enhancement of Shape-Reconfigurable Mushroom-Shaped Microstructures

Hyunwook Ko

Department of Mechanical Engineering

Graduate School of UNIST

2020

Adhesion Enhancement of Shape-Reconfigurable Mushroom-Shaped Microstructures

Hyunwook Ko

Department of Mechanical Engineering

Graduate School of UNIST

Adhesion Enhancement of Shape-Reconfigurable Mushroom-Shaped Microstructures

A thesis

submitted to the Graduate School of UNIST

in partial fulfillment of the

requirements for the degree of

Master of Science

Hyunwook Ko

12/09/2019

Approved by

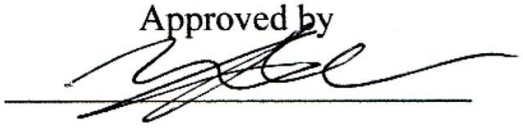

Advisor

Hoon Eui Jeong

Adhesion Enhancement of Shape-Reconfigurable Mushroom-Shaped Microstructures

Hyunwook Ko

This certifies that the thesis of Hyunwook Ko is approved.

12/09/2019

signature

Advisor: Hoon Eui Jeong

signature

Prof. Sung Youb Kim

signature

Prof. Hyung Wook Park

Abstract

Dry adhesives with mushroom-shaped microstructures, inspired by structures on feet of gecko lizard, have been used in various fields such as climbing robotics, precision transportation, and clean manufacturing due to their unique adhesion property originated from van der Waals force under conformal contact. The dry adhesive microstructures are usually composed of elastomers with fixed Young's modulus such as polydimethylsiloxane (PDMS) or polyurethane. However, the dry adhesives microstructures in previous studies cannot conformally contact to surfaces with micro-scale roughness. Although dry adhesives comprised of the elastomers having relatively low Young's modulus were previously suggested to overcome the limitation, problems still remained unsolved as it is hard to exploit elastomers with low elastic modulus for adhesive microstructures due to their low structural stability and weak adhesion.

To this end, we propose the mushroom-shaped microstructure comprised of the shape-reconfigurable polymer as a breakthrough to dramatically enhance the adhesion onto rough surfaces. The elastic modulus of the shape-reconfigurable polymer can be actively tuned by external stimuli such as heat, electricity, light, and water. Under the appropriate stimuli, the elastic modulus of the shape-reconfigurable polymers can be decreased, then the adhesive microstructure made of the shape memory polymer can conformally contact to rough surfaces, as in the case of elastomers with low modulus (adaptation). After that, the elastic modulus of the shape-reconfigurable polymers can be recovered to their original state by eliminating the stimuli for enhanced adhesion (fixation). Moreover, the shape-reconfigurable polymers enable reversible use of dry adhesive microstructures even after severe deformation, due to their shape recovery property.

The first part covered in this thesis is the background to set a blend of elastic polyurethane acrylate (e-PUA) and polycaprolactone (PCL) as a new material for dry adhesive microstructures. The material properties and advantages of the e-PUA/PCL blend were introduced.

The second part of the research is the experimental observations and measurements. The paper and line pattern substrates are set as surfaces for adhesion, as representatives of an irregular surface and a regular surface, respectively. The adhesion enhancement procedures including adaptation and fixation are experimentally observed using scanning electron microscopy (SEM) and optical microscopy (OM). The elastic moduli of the e-PUA/PCL blend with various mixing ratios were measured and the optimal ratio for the adhesion enhancement was defined.

The thirdly covered part is about the theoretical investigation of the adhesion enhancement mechanism. The analyses were conducted under the hypothesis, which is a difference in the contact

area between adapted and non-adapted states causes dissimilarity in adhesion. To validate this hypothesis, theoretical adhesion force was calculated with a formula of the Johnson-Kendall-Roberts (JKR) adhesion model. In addition, finite element analysis (FEA) was carried out to calculate the contact area between the mushroom-shaped microstructures and the substrates. Using these results, a relation formula between the adhesion strengths and Young's modulus was defined. The theoretical values of adhesion were compared to the experimental measurements to validate the reliability of the analyses.

In total, the adhesion enhancement utilizing mushroom-shaped microstructures made of the shape-reconfigurable polymer was experimentally demonstrated and its mechanism was theoretically analyzed in this thesis. It was shown that the adhesive microstructures comprised of the shape-reconfigurable polymer could enhance adhesion with maximization of contact area and recovery of high Young's modulus due to the elastic modulus-tunable property.

Contents

List of Figures

List of Tables

Nomenclature

Abbreviations

ALE	Arbitrary Lagrangian-Eulerian
e-PUA	Elastic polyurethane acrylate
FEA	Finite element analysis
FEM	Finite element method
JKR	Johnson-Kendall-Roberts
OM	Optical microscopy
PCL	Polycaprolactone
PDMS	Polydimethylsiloxane
PUA	Polyurethane acrylate
SBS	Styrene-butadiene-styrene tri-block copolymer
SEM	Scanning electron microscopy

List of symbols

Symbol	Quantity	Unit
F	Adhesion force	[N]
a	Radius of the contact area	[m]
E_f	Young's modulus of adhesive in fixation state	[Pa]
W	Work of adhesion between the adhesive microstructure and the substrate	[J/m^2]
v	Poisson's ratio of adhesive	
γ^d	Dispersion components of surface energy	[J/m^2]
γ^p	Polar components of surface energy	[J/m^2]
A	Contact area	[m^2]
P	Pull-off strength	[Pa]

r	Radius of the main pillar	[m]
E	Young's modulus of adhesive in adaptation state	
p	Constants of the approximation for the paper substrate	
l	Constants of the approximation for the line pattern substrate	

1. Introduction

1.1 Previous researches

1.1.1 Limitations of previous bio-inspired adhesives

In nature, gecko lizards [1-5] and some species of beetles like *Gastrophysa viridula* [6-9] have fascinating ability to walk and climb on the wall or rough surfaces like plant leaves. The secret of the ability was the micro-scaled structures that look like minute hair shrouding at the feet of gecko lizard [1-5] and beetles as shown in figure 1 and figure 2 [6-10]. The microstructures similar to spatula can stick to some substrates by van der Waals force [1-5, 11], which is an interactive force between molecules that occurred by dipoles which means a molecule has an electric field due to uneven distribution of positive and negative charges in atoms [12].

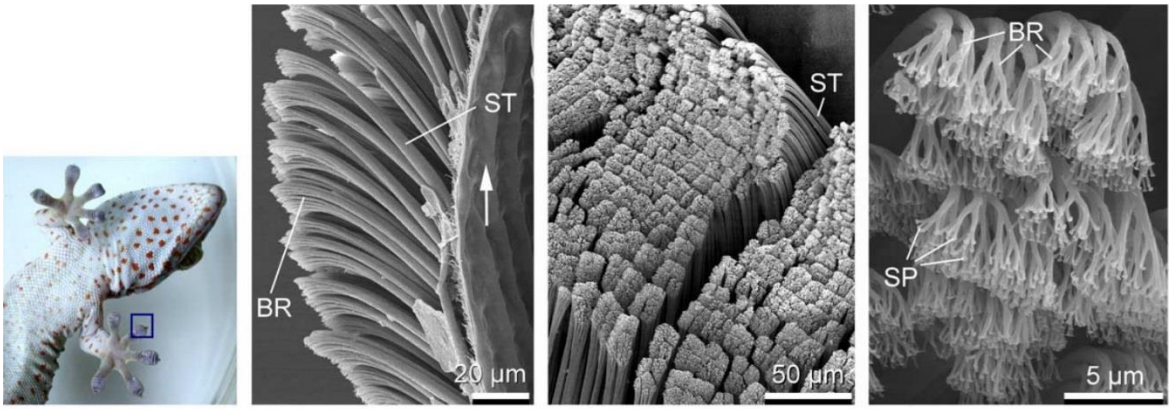

Figure 1 The hierarchical adhesive structures of Gekko gecko. A toe of gecko contains hundreds of thousands of setae and each seta contains hundreds of spatulae. (a) and (b): scanning electron micrographs of rows of setae at different magnifications and (c): spatulae, the finest terminal branches of seta. ST: seta; SP: spatula; BR: branch [1].

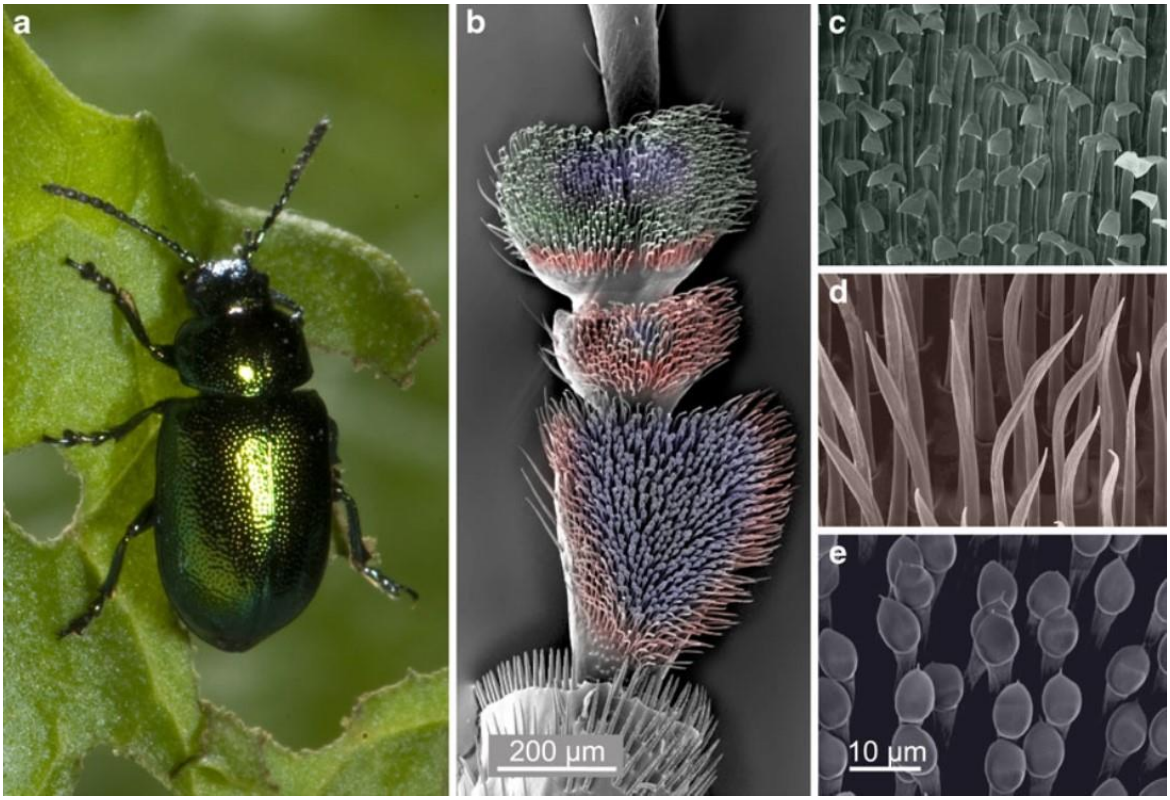

Figure 2 (a) Adhesive pad morphology of a male dock beetle G. viridula. (b) Three tarsal pads of the hind leg. (c)–(e) Adhesive hair morphologies, presented to the same scale: (c) spatula-tipped, (d) pointed and (e) discoidal. The color-coding indicates the distribution of seta types across the tarsal pads [6].

Inspired by the natural adhesive microstructures that maximize van der Waals force for high adhesion, a mushroom-shaped microstructure has been proposed in previous research. The mushroom-shaped pillar has a strong pull-off strength because it has a rounded tip shape to avoid stress concentration [13-15].

To investigate the adhesion mechanism of the adhesive microstructures, a flat punch and mushroom-shaped model were previously reported [16]. Based on the research, the mushroom-shaped microstructure with the optimal tip thickness has high adhesion strength whereas that with too thin or thick tip and the flat punch cannot adhere strongly due to the stress singularity.

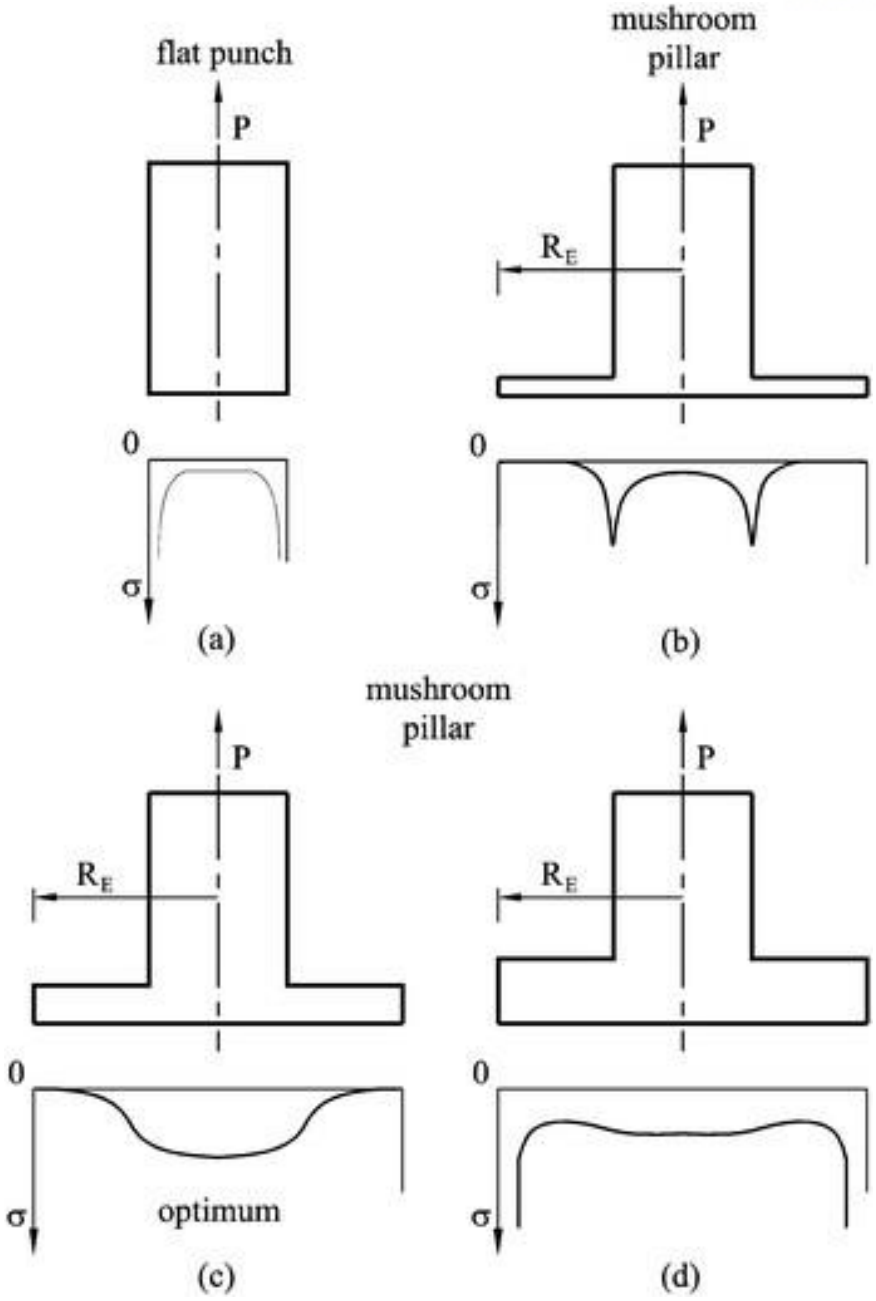

Figure 3 The stress distribution in case of an (a) flat punch, and for a mushroom-shaped pillar for three different thicknesses of the plate: (b) thin, (c) medium (d) and thick. The presence of the plate eliminates the stress singularity of the flat punch at r ≈ R. The stress peak in the mushroom pillar at r ≈ R will gradually vanish as the plate thickness t is increased up to its optimal value (c) [16].

Meanwhile, the most commonly used material to fabricate the mushroom-shaped microstructure is polydimethylsiloxane (PDMS) [17-21] as PDMS has many advantages such as its easiness to manufacture, optical transparency, relatively cheap price, biocompatibility, flexibility, and no residue remaining [22-27]. However, the microstructures made of PDMS exhibit weak adhesion on rough

substrates such as skin, paper, and Al foil because the microstructures cannot have conformal contact as the elastic modulus of PDMS is too high [28-33]. This is because the non-conformal contact disturbs the sufficient work of van der Waals force. Therefore, new materials had been required to achieve adhesive for more complicated substrates.

As the biggest problem of PDMS is that it cannot follow the rough surface due to its high modulus, many researchers have been studied about elastomers with relatively lower Young's modulus. The microstructures made of elastomer with low Young's modulus is able to follow a rough surface better than those made of PDMS and maximize the contact area with a substrate. However, elastomers with low elastic modulus possess two other problems of structural instability and easy crack propagation as well. Besides, the material with low elastic modulus is difficult to use in the fabrication of microstructures. The tips of mushroom-shaped pillars are severely distorted when the elastic modulus is lower (~1.5 MPa) than normal PDMS with 10% of crosslinker concentration (~2.0 MPa) [34]. In addition, the unwanted crack propagation diminished the adhesion. Therefore, it can be noted that low Young's modulus directly lessens the adhesion (figure 4) [34-36].

Based on the previous studies, it is confirmed that mushroom-shaped microstructures with low elastic modulus are advantageous in conformal contact to rough surfaces, whereas those with high elastic modulus have merits in preventing crack propagation. Therefore, the material with elastic modulus-tunability is a highly potential candidate to enhance the adhesion of the microstructures.

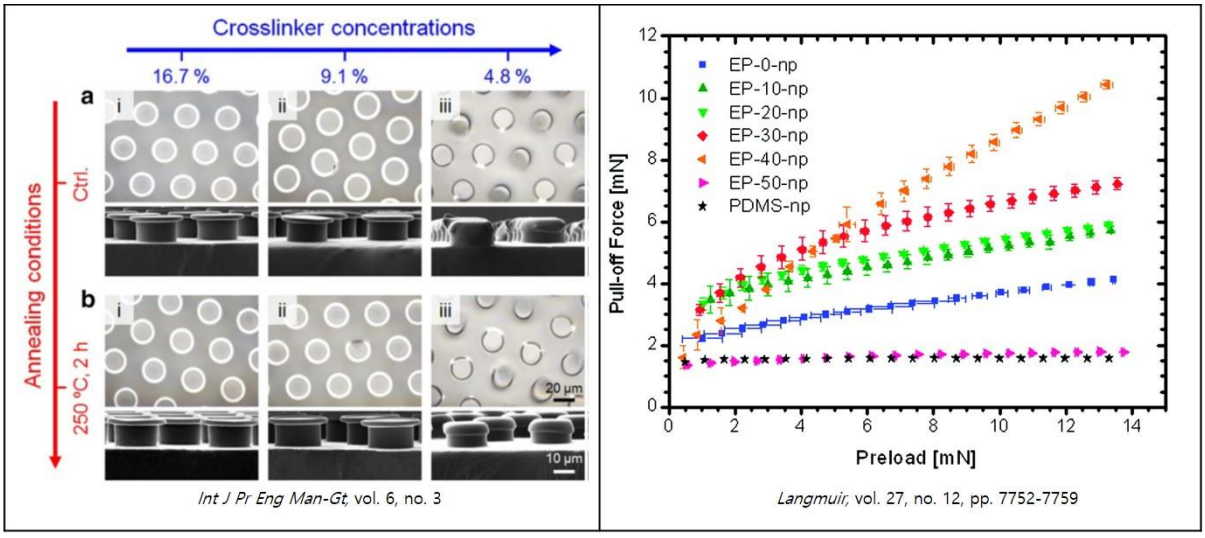

Figure 4 Previous research on the adhesive microstructure made of low elastic modulus [34, 36].

1.1.2 Shape-reconfigurable polymers as solutions

As a solution for limitations of traditional elastomers explained above, a shape-reconfigurable polymer or shape memory polymer can be adopted because it is possible to alter its Young's modulus by various stimuli [37]. The shape-reconfigurable polymers have several triggers such as water, light, heat, pH, and solvent as shown in figure 5. The features of shape-reconfigurable polymers such as large deformation inducing conformal contact, maintenance of deformed state lowering crack propagation before stimulated, and shape memory effect by the stimulus are presented in figure 6 [38].

Tunable elastic modulus is important to enhance the adhesion because low Young's modulus enables conformal contact and high modulus validates both structural stability and reducing crack propagation. Additionally, a shape memory effect of the shape-reconfigurable polymer enables the reversible use of a mushroom-shaped pillar as its shape can be recovered after the deformation.

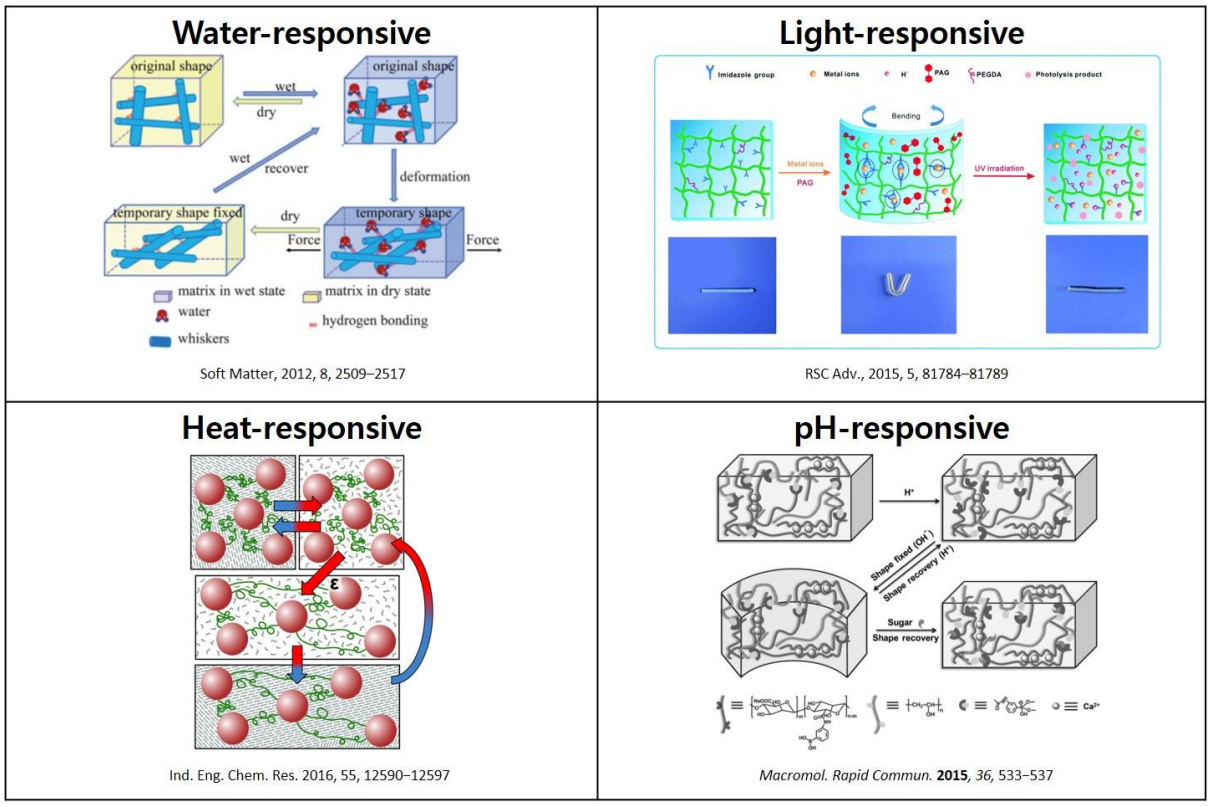

Figure 5 Four types of shape memory polymers possessing triggers such as water, light, heat and, pH [39-42].

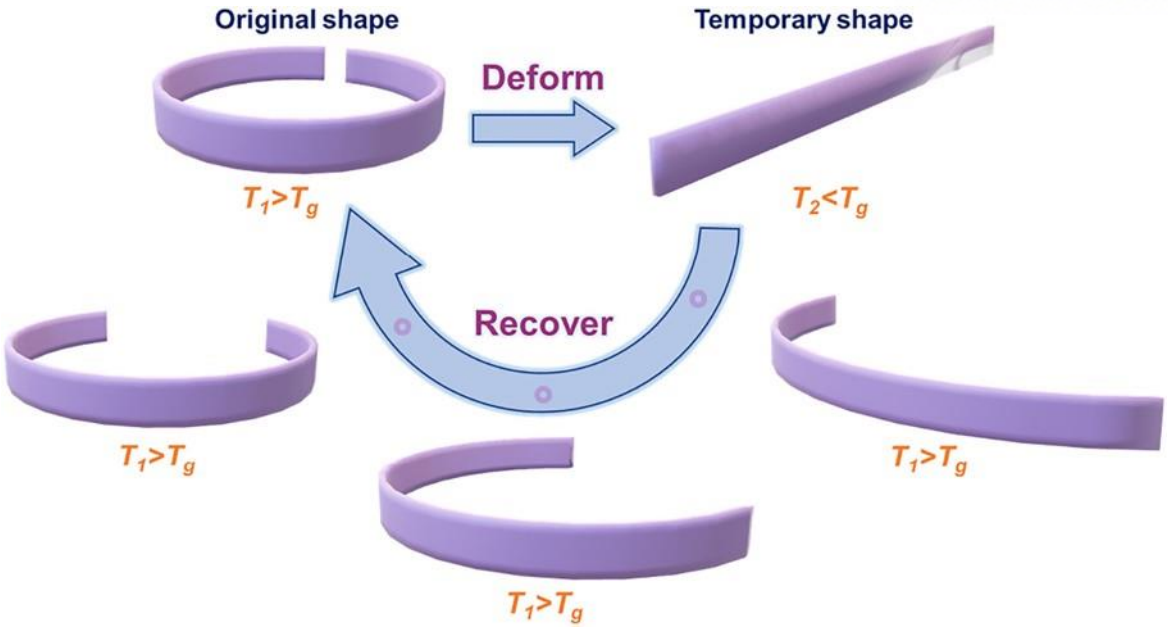

Figure 6 Scheme diagram of deformation and recovery process in the fold-deploy tests of DLP-printed SMPs. [38].

Figure 7 also shows an example of shape memory polymers responsive to heat [43], which is a blend of two independent materials styrene-butadiene-styrene tri-block copolymer (SBS) and polycaprolactone (PCL) unlike other shape memory polymers formed by chemical bonds. SBS is a common elastomer and PCL works as a switch to tune the material property of the blend with the aid of its low melting temperature. The blend becomes soft by applying heat to melt PCL then the blend can be easily deformed. At the deformed state, the blend maintains its deformed shape if it is cooled below the melting point of PCL. After that, the blend recovers its original shape by heating as SBS is an elastomer with recovering disposition.

The shape-reconfigurable polymers enabling to tune their Young's modulus with stimuli (figure 8) are appointed a strong candidate material for a mushroom-shaped pillar and the solution for limitations of conventional elastomers. The phenomenon that the mushroom-shaped pillar conformally contacts to surfaces by lowering Young's modulus and becomes firm by recovering its modulus is called adaptation and fixation, respectively. These two procedures give the solution to overcome the limitations [44, 45]. With the reversible tuning of elastic modulus, the adhesion of the mushroom-shaped pillar can be considerably enhanced. In addition, the structural stability and shape recovery for reversible adhesion are also extra benefits of using the shape-reconfigurable polymers.

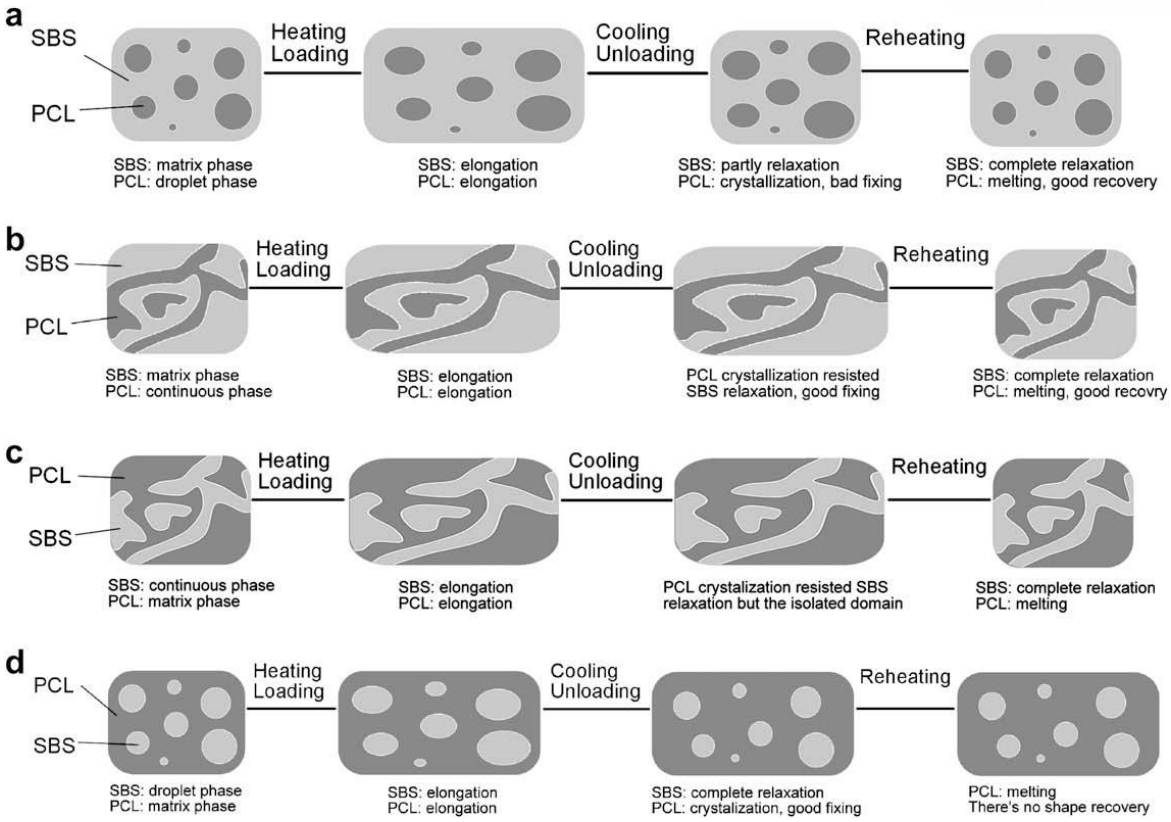

Figure 7 Schematic figures of the shape memory mechanism of elastomer/switch polymer blends concluded from SBS/PCL blend [43].

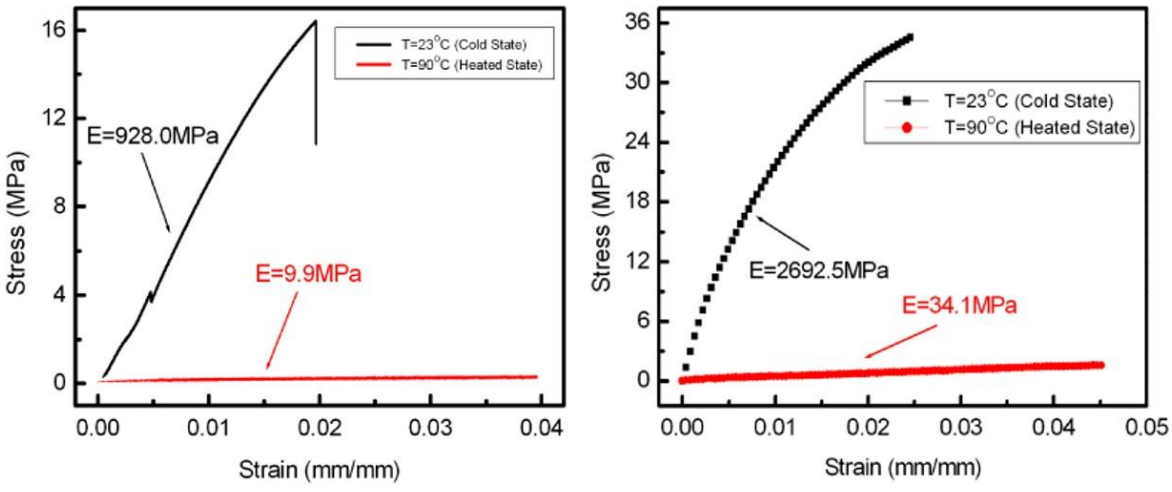

Figure 8 Experimental curves of engineering stress versus strain of SMP (left) and SMPC (right) [46].

1.2 Research purpose and outline

The purpose of this research is to propose the adhesion enhancement mechanism using shape-reconfigurable polymer by experiments and theoretical analyses as a way of going beyond the limitations of existing adhesive microstructures such as low adhesion on rough surfaces and low structural stability. A detailed outline of the research to achieve the purpose is as follows:

Firstly, experimental results to ascertain the adhesion enhancement mechanism of the mushroom-shaped pillar composed of the shape-reconfigurable polymer will be suggested in chapter 2. The adhesion enhancement property will be substantiated by the scanning electron microscopy (SEM) exhibiting images of the mushroom-shaped pillars after the adaption and fixation. The shape recovery characteristic will be certified by the sequential optical microscopy (OM) displaying the real-time images of the shape recovery process by heat-stimulus. Variations of Young's moduli with respect to heat and the mixture ratio of a blend of elastic polyurethane acrylate (e-PUA) and polycaprolactone (PCL) will be portrayed to discover the most appropriate ratio for the experiment. The difference in pull-off strength between adapted and non-adapted microstructures will be compared to each other at the end of chapter 2.

Secondly, the theoretical background of adhesion will be proposed in chapter 3 to prepare the theoretical analysis of the adhesion enhancement mechanism of the mushroom-shaped pillar comprised of the shape-reconfigurable polymer. The formula of theoretical adhesion obtained by the Johnson-Kendall-Roberts (JKR) model will be modified in a suitable form to apply to this study in chapter 3.

Thirdly, the theoretical calculation of the pull-off strength with the finite element analysis (FEA) will be accomplished and compared to experimental results in chapter 4. The theoretical contact area between a single mushroom-shaped pillar and the substrates will be calculated by FEA as Young's modulus changes and the correlation between the contact area and Young's modulus will be found out. Subsequently, the theoretical pull-off strength will be calculated by using the modified formula of adhesion and the correlation between the contact area and Young's modulus. The comparison of theoretical and experimental results will be conducted to verify the accuracy of theoretical analysis about the adhesion enhancement mechanism at the end of chapter 4.

2. Experimental result: Adhesion enhancement using e-PUA/PCL blend

Among many shape memory polymers, we chose the blend of e-PUA and PCL to fabricate the mushroom-shaped pillar because it has low Young's modulus (~0.6 MPa) when it is heated to ~70 °C for adaptation while it has high Young's modulus (~210 MPa) when it is cooled for fixation. To verify these characteristics, the mushroom-shaped pillars made of the e-PUA/PCL blend were pressed to the paper and line pattern substrates then the results were observed using SEM (figure 9). The mushroom-shaped pillars were largely and conformally deformed by pressing, which well demonstrates the adaptability of shape memory polymer. In addition, the fixation of shape memory polymer that can maintain its shape by raising Young's modulus is well demonstrated in the figure as the pre-deformed shapes are preserved without bending of main pillars. Furthermore, the ability to recover original shape under heating, which is shape memory capability, was confirmed experimentally with the paper substrate and line pattern substrate, respectively (figure 10 and 11). The shape of the pillars was recovered quickly within 20 seconds by heating.

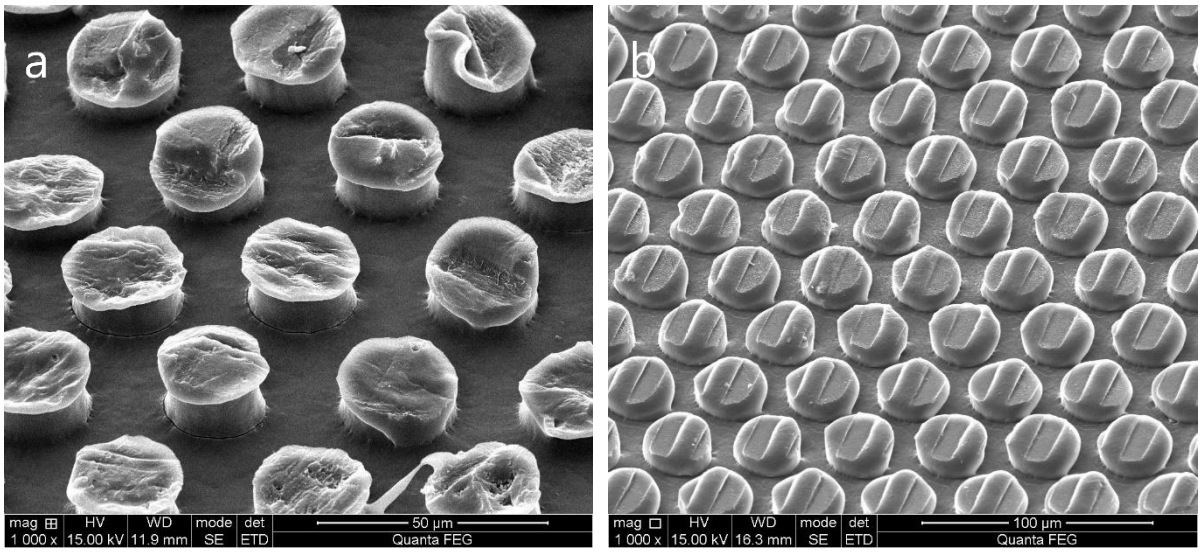

Figure 9 SEM images of mushroom-shaped pillars made of the blend of e-PUA and PCL after adapted to two substrates (a) paper substrate and (b) line pattern substrate.

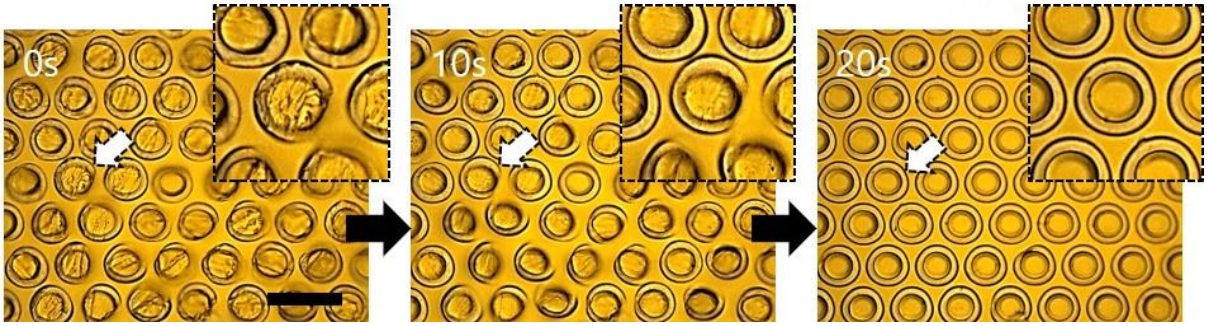

Figure 10 Real-time OM images describing the mushroom-shaped pillars recovering their shape from the deformed state after adapted to the paper substrate. It can be seen that recovery time is very fast (~20 s) after stimulated by heat. Scale bar is 40 μm.

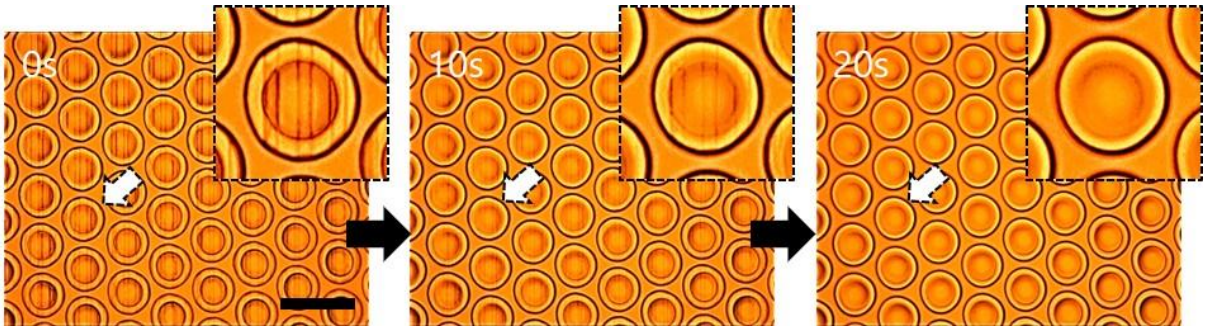

Figure 11 Real-time OM images describing the mushroom-shaped pillars recovering their shape from the deformed state after adapted to the line pattern substrate. It can be seen that recovery time is very fast (~20 s) after stimulated by heat. Scale bar is 40 μm.

After the validation of the material properties of the e-PUA/PCL blend, the elastic moduli with the different mixing ratios of the blend were measured as shown in figure 12. The mixture ratios written in the legend indicate the weight of e-PUA to the weight of PCL. As the portion of e-PUA in the blend decreases, Young's modulus increases without heat stimulus, whereas the modulus decreases with heating to 70 °C. This is because PCL alternating between solid and liquid has more influence on Young's modulus than e-PUA with fixed Young's modulus. From the experimental results, it is confirmed that the e-PUA/PCL blend with a mixture ratio of 1:1 is the most suitable blend to maximize the adhesion enhancement effect because the gap between the elastic moduli with and without heating stimulus is the largest among three different mixing ratios. For this reason, the mushroom-shaped pillars with the mixture ratio of 1:1 were adopted. Consequently, the adhesion strength of the mushroom-shaped pillar with the designated mixing ratio was measured with respect to the paper and line-patterned substrates at the preload of 10kPa (figure 13). The pull-off strength under the adapted condition was significantly higher than the non-adapted condition.

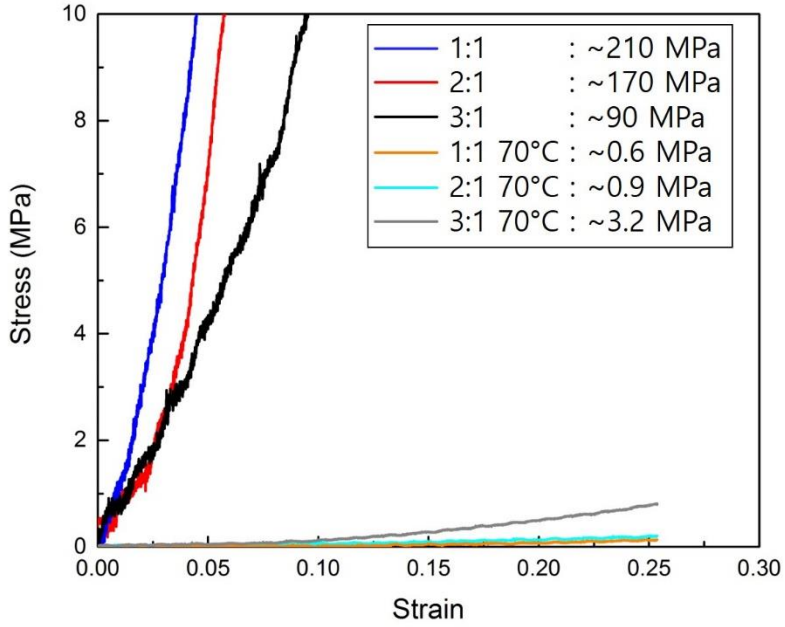

Figure 12 Experimental curves of stress versus strain of the blend of e-PUA and PCL according to mixture ratio (e-PUA:PCL in legend box) and temperature (room temperature and 70 °C).

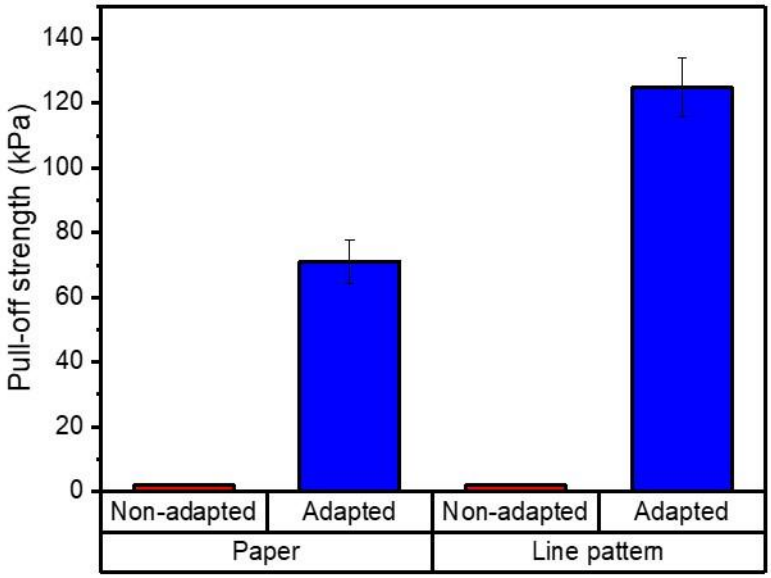

Figure 13 Experimental measurement of pull-off strength for adapted and non-adapted conditions according to paper and line pattern the substrate.

The SEM & OM images and the experimentally measured pull-off strength of the mushroom-shaped pillars made of the blend of e-PUA and PCL have been presented and confirmed adhesion enhancement phenomena in this chapter. The fabricated heat-responsive mushroom-shaped pillars exhibited the characteristics of conformal deformation along surfaces by heating (adaptation), solidification after deformation by cooling (fixation), and shape recovery by heating again.

3. Theoretical analysis: Adhesion enhancement mechanism

To theoretically analyze the adhesion force according to the change in the elastic modulus, following two numerical calculations are required: 1) the adhesion-contact area relation formula and 2) contact area defined by the elastic modulus through the finite element method (FEM), which are introduced in chapter 3.1 and 3.2, respectively. Theoretical adhesion strengths and comparisons of analyzed theoretical results with previously obtained experimental measurements will be dealt with in chapter 3.3 and 3.4, respectively. The preliminary setup procedure of all conditions for the theoretical analyses is described in chapter 3.5.

3.1. Theoretical backgrounds

Johnson, Kendall, and Roberts formulated the JKR theory and the model of contact mechanics that describes the effects of contact pressure and adhesion with respect to contact area when two elastic spheres attached to each other. The JKR adhesion model is shown in figure 14 [47]. Among the various cases of JKR models, the description in Figure 14 is appropriate to apply to our adhesion system because the adhesive domain has a lower elastic modulus than the substrates domain in this study.

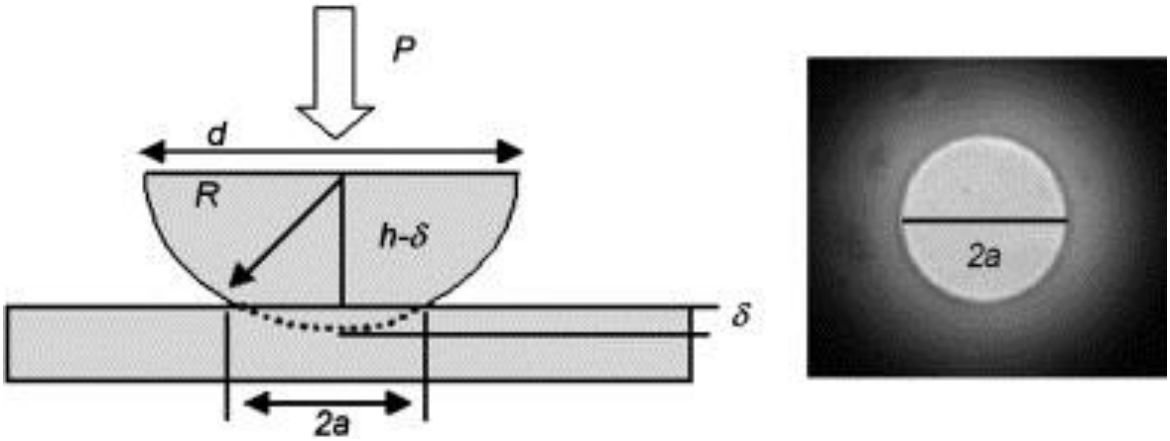

Figure 14 Schematic representation of an elastic semi-sphere and a flat sheet in contact under a load P (left), along with an image of the contact area (right) **[47]**.

The adhesion force formula of JKR model with spherical adhesive is given as [48, 49]:

$$F = \sqrt{\frac{8\pi a^3 E_f W}{1-\nu^2}} \quad (1)$$

where a is the radius of contact area, E_f is Young's modulus of adhesive in fixation state, W is the work of adhesion between the adhesive microstructure and the substrate, and v is the Poisson's ratio of adhesive. The work of adhesion W can be obtained by the geometric mean of dispersion and polar components of surface energy as follows [50]:

$$W = 2\sqrt{\gamma_1^d \gamma_2^d} + 2\sqrt{\gamma_1^p \gamma_2^p} \tag{2}$$

where γ^d and γ^p are is dispersion and polar components of surface energy, respectively. The formula (1) is required to be modulated because the contact region of this study is not a perfect circle. A new parameter, contact area A can be expressed as

$$A = \pi a^2 \tag{3}$$

By the equation 3, the radius of the contact area a can be expressed as by the contact area A:

$$a = \sqrt{\frac{A}{\pi}} \tag{4}$$

Consequently, equation 1 modulated by inserting equation 4 is given by:

$$F = \sqrt{\frac{8E_f W}{1-\nu^2}} \cdot \frac{A^{0.75}}{\pi^{0.25}} \tag{5}$$

This is the formula of theoretical adhesion force depending on Young's modulus, the surface energy, Poisson's ratio, and the contact area. Lastly, dividing the equation 5 by the area of a unit cell of the mushroom-shaped pillar array is required to obtain the final formula with a unit of Pa, which is the unit of experimental measurement of adhesion strengths. The final formula of the adhesion strength is expressed as:

$$P = \frac{A^{0.75}}{\pi^{0.25} r^2} \sqrt{\frac{E_f W}{24(1-\nu^2)}} = \frac{A^{0.75}}{\pi^{0.25} r^2} \sqrt{\frac{E_f (2\sqrt{\gamma_1^d \gamma_2^d} + 2\sqrt{\gamma_1^p \gamma_2^p})}{24(1-\nu^2)}} \tag{6}$$

This is the formula of pull-off strength where r is the radius of the main pillar.

As indicated in equation 6, increasing the contact area (A) and elastic modulus (E_f) is critical for the adhesion enhancement. This verifies that the adaptation (maximizing the contact area by lowering the elastic modulus) and fixation (recovering the elastic modulus after the adaptation) procedure is the main mechanism to enhance the adhesion of the mushroom-shaped microstructures made of the shape-reconfigurable polymer.

3.2 Finite element analysis

This chapter aims to establish the relation equation between the contact area and the elastic modulus. The contact areas between the substrates (paper and line pattern) and the single mushroom-shaped pillar with various elastic moduli were numerically analyzed using Abaqus.

3.2.1 Contact area analysis on the paper substrate

The mushroom-shaped pillars with various Young's modulus from 0.1 MPa to 500 MPa were set to contact with the paper substrate by the pressure of 10 kPa, as shown in figure 15. The scale bar refers to mechanical strain. The non-blue regions of the mushroom-shaped pillar indicate the deformed regions where mechanical strain exists. As shown in figure 15(a) – 15(e), it can be immediately seen that the contact area between the mushroom-shaped pillar and the paper substrate decreases as Young's modulus increases. The calculated values of the contact area are 352.961 μm^2, 60.648 μm^2, 10.124 μm^2, 2.36 μm^2, and 0.966 μm^2 when Young's modulus is 0.1 MPa, 1 MPa, 10 MPa, 100 MPa, and 500 MPa, respectively.

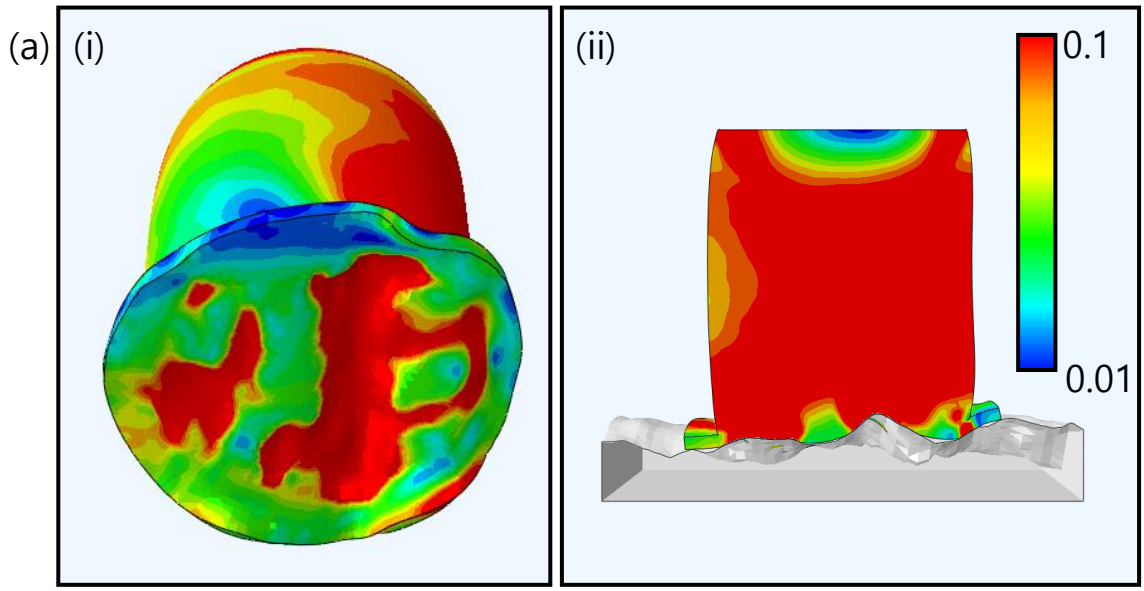

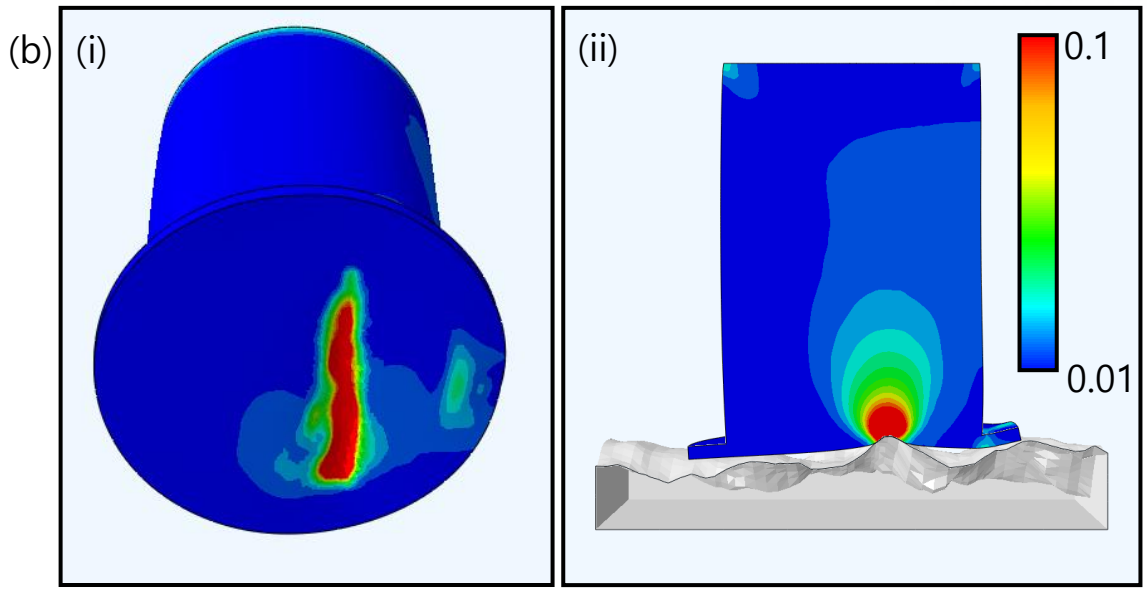

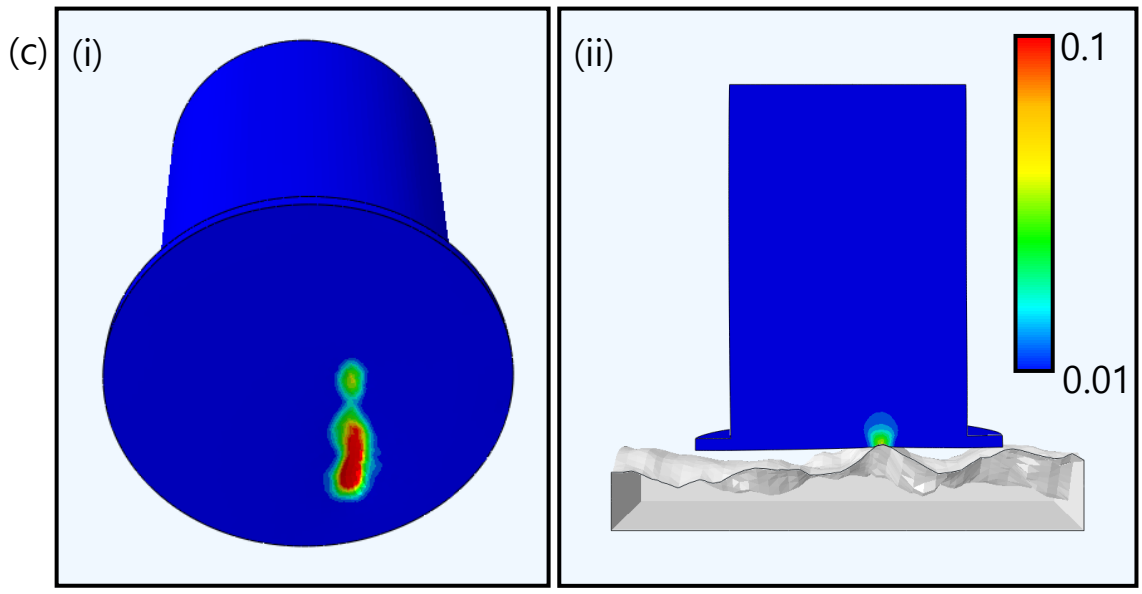

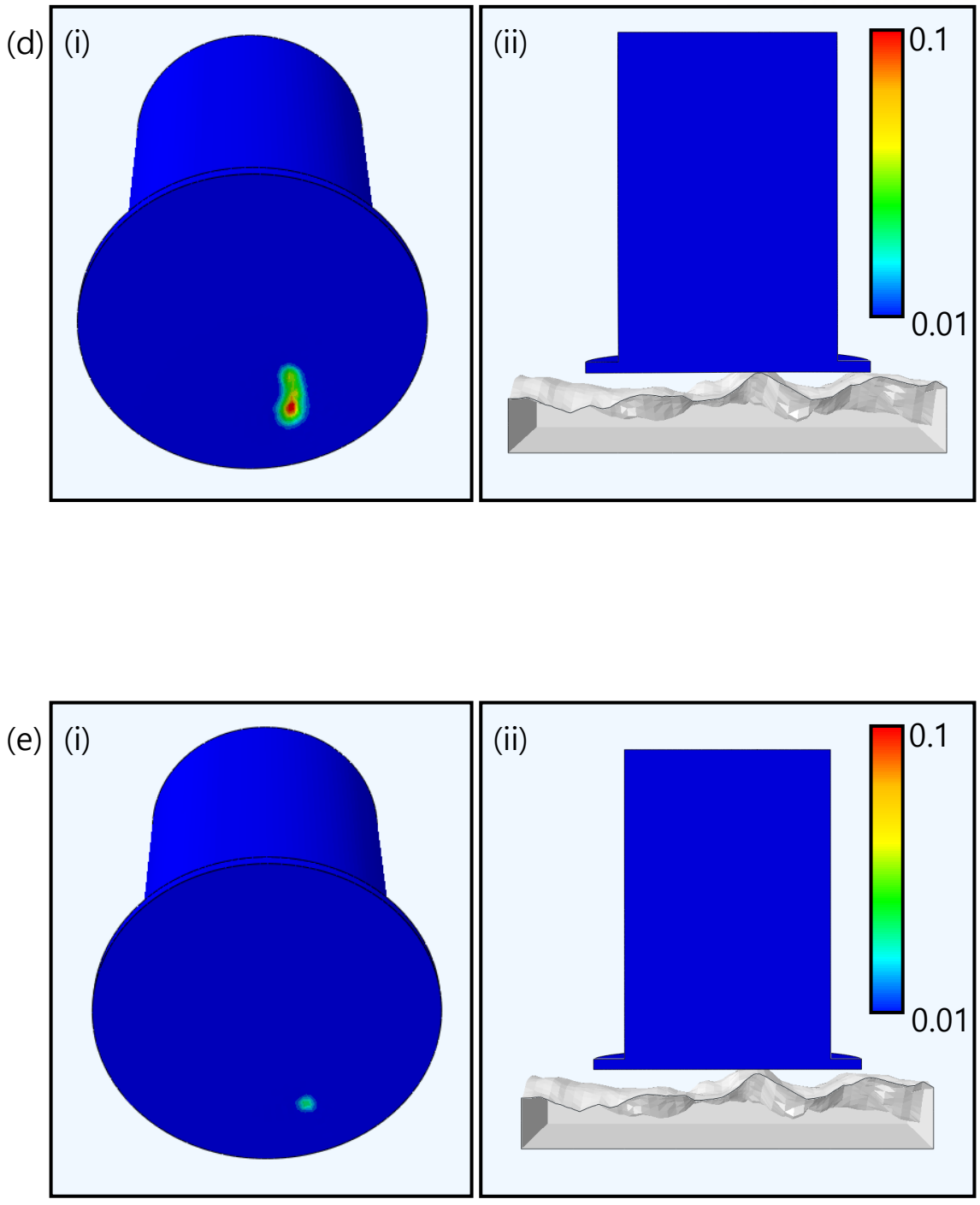

Figure 15 The FEA result on paper of mushroom-shaped pillar describing strain region when Young's modulus is (a) 0.1 MPa (b) 1 MPa (c) 10 MPa (d) 100 MPa and (e) 500 MPa. (i) The left picture of each case shows the bottom of the pillar and (ii) the right picture shows a cross-section of the pillar. Scale bar indicates true strain.

Using the calculated contact areas, a relation between the contact area and the elastic modulus was defined with mathematical approximation fitting the power-law as described in figure 16. Young's modulus in the x-axis is expressed as a common logarithms scale for high clarity and visibility.

The equation of the approximation governing the relation between the contact area and the elastic modulus is given by:

$$A = p_1 E^{p_2} \tag{7}$$

where A is the contact area, E is Young's modulus of adhesive in adaptation state, p_1 is 60.61527 and p_2 is -0.76515.

Based on the derived equation, the numerically predicted contact areas of the mushroom-shaped pillar made of predefined e-PUA/PCL blend (1:1 in mixing ratio) can be given by 89.604 μm^2 and 1.013 μm^2 for thermally stimulated state (heating, 70 °C / Young's modulus: 0.6 MPa) and original state (room temperature, 20 °C / Young's modulus: 210 MPa), respectively.

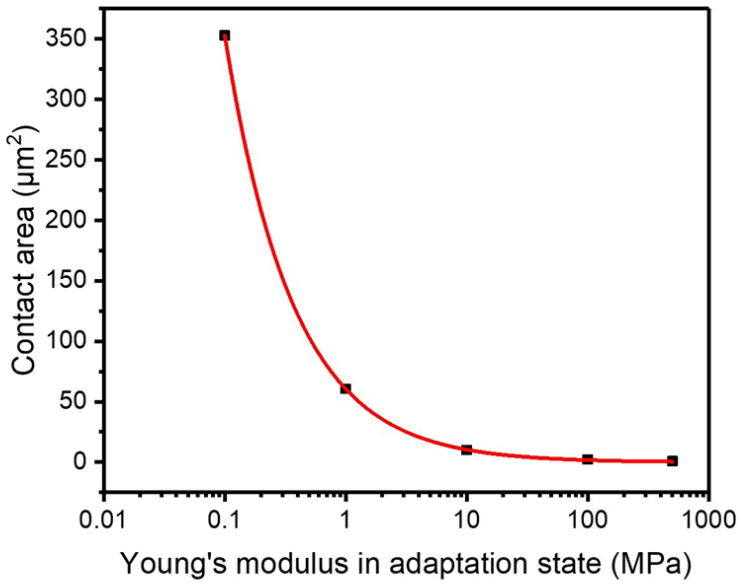

Figure 16 A graph describing the correlation between contact area versus Young's modulus of the mushroom-shaped pillar when the substrate is paper.

3.2.2 Contact area analysis on the line pattern substrate

The mushroom-shaped pillars with various Young's modulus from 0.1 MPa to 500 MPa were set to contact with the line pattern substrate by the pressure of 10 kPa, as shown in figure 17. The overall tendency of the result is highly similar to that on the paper substrate. The contact area between the mushroom-shaped pillar and the line pattern substrate decreases as Young's modulus increases. The calculated values of the contact area are 438.59 μm^2, 229.921 μm^2, 90.488 μm^2, 17.336 μm^2, and 3.3364 μm^2 when Young's modulus was 0.1 MPa, 1 MPa, 10 MPa, 100 MPa, and 500 MPa, respectively.

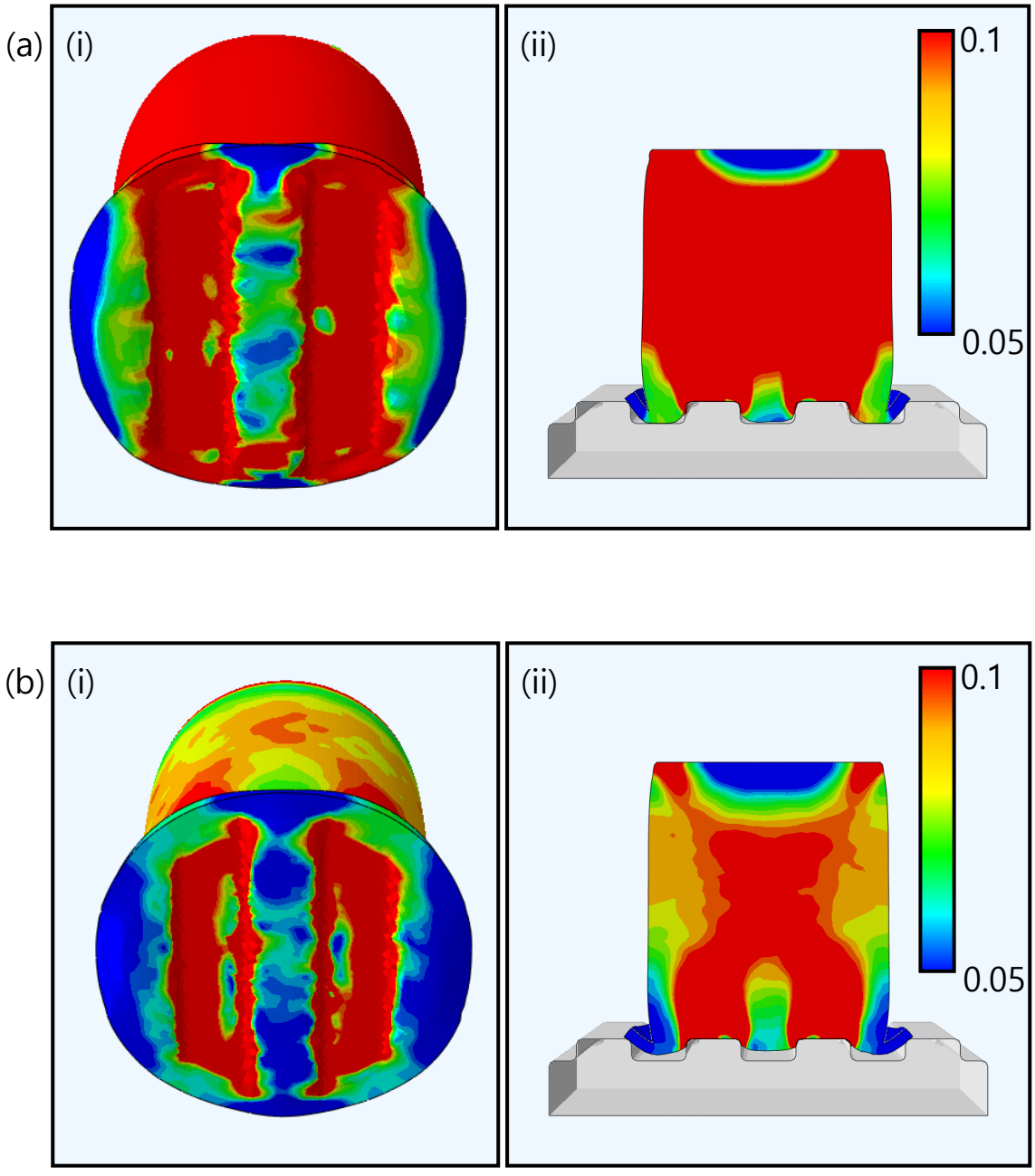

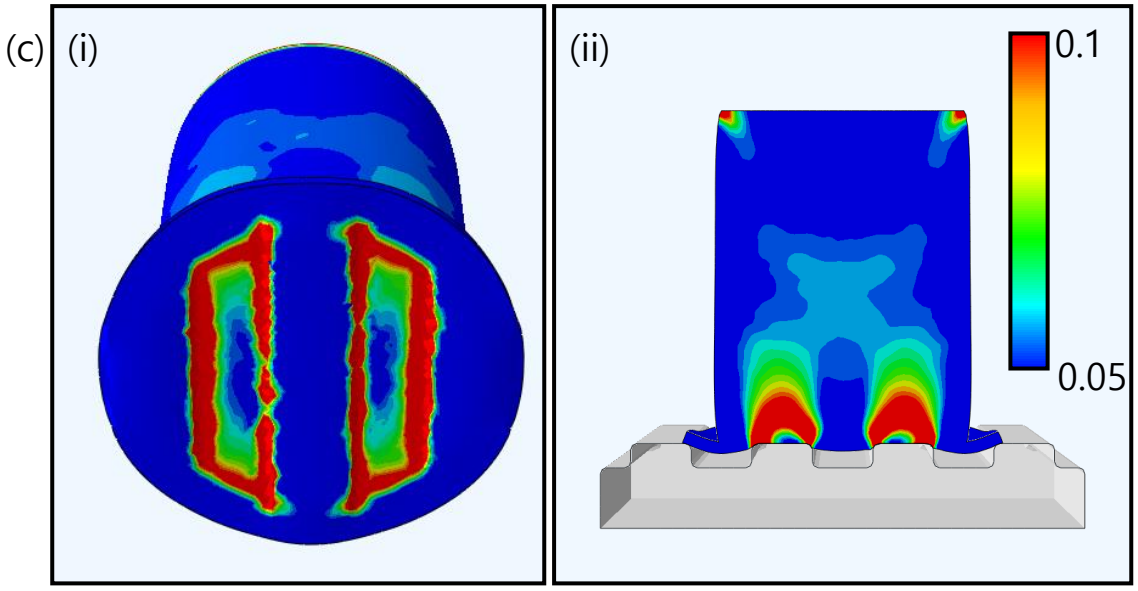

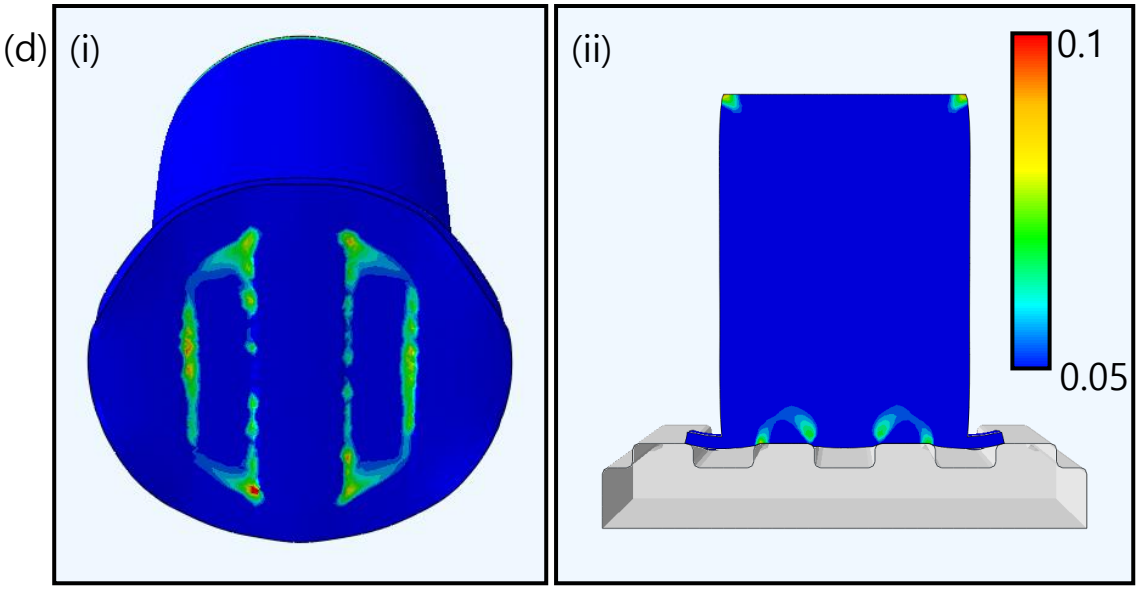

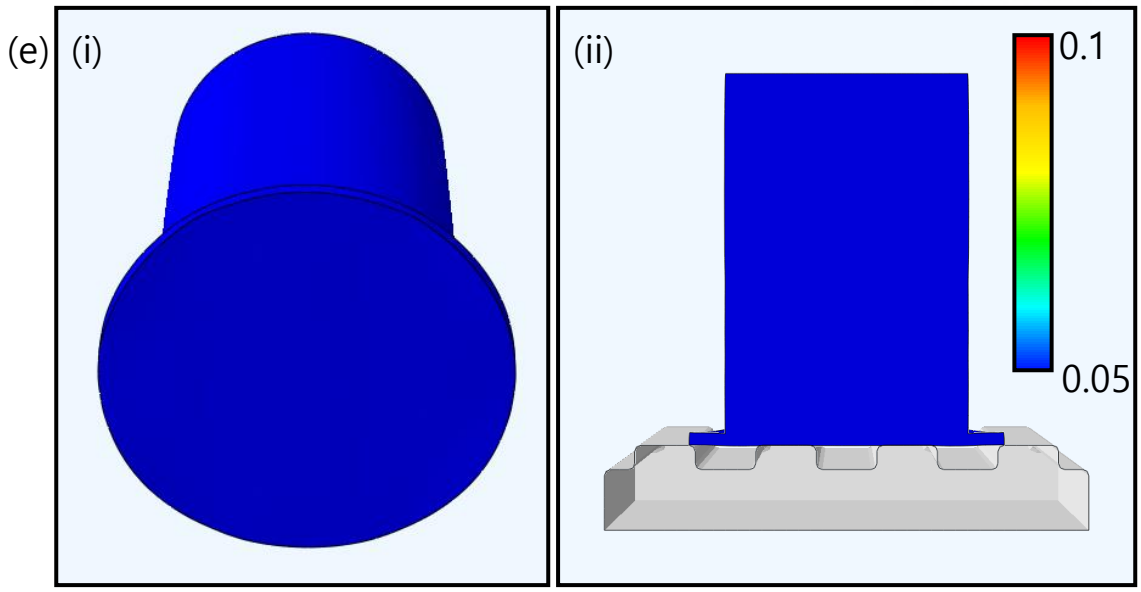

Figure 17 The FEA result on the line pattern substrate of mushroom-shaped pillar describing strain region when Young's modulus is (a) 0.1 MPa (b) 1 MPa (c) 10 MPa (d) 100 MPa and (e) 500 MPa. (i) The left picture of each case shows the bottom of the pillar and (ii) the right picture shows a cross-section of the pillar. Scale bar indicates true strain.

Again, the relation between the contact area of the mushroom-shaped pillar on the line pattern substrate and Young's modulus was defined with mathematical approximation fitting, as shown in figure 18. Young's modulus in the x-axis is expressed as a common logarithms scale. The equation of the approximation governing the relation between the contact area and the elastic modulus is given by:

$$A = l_1 E^{l_2} \quad (8)$$

where l_1 is 203.35552 and l_2 is -0.34183.

Based on the derived equation, the numerically predicted contact areas of the mushroom-shaped pillar made of predefined e-PUA/PCL blend (1:1 in mixing ratio) can be given by 242.153 μm^2 and 32.693 μm^2 for thermally stimulated state (heating, 70 °C / Young's modulus: 0.6 MPa) and original state (room temperature, 20 °C / Young's modulus: 210 MPa), respectively.

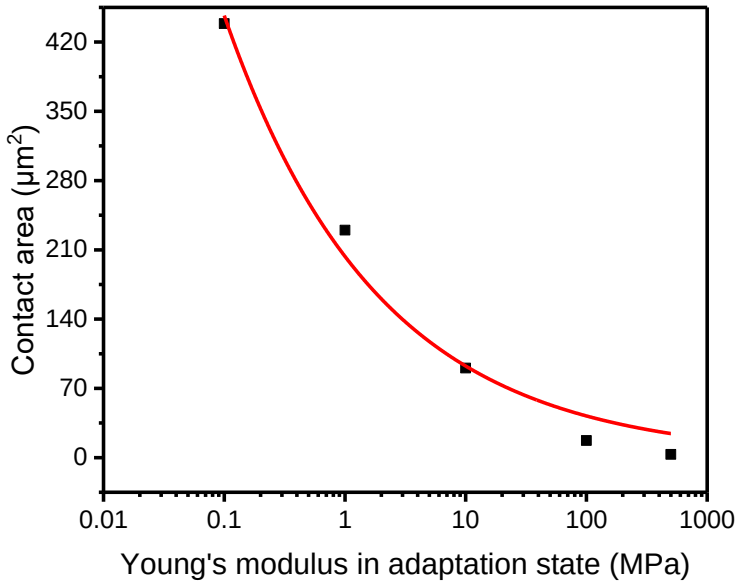

Figure 18 A graph describing the correlation between contact area versus Young's modulus of the mushroom-shaped pillar when the substrate is the line pattern surface.

As shown in figure 16 and 18, the relations between contact areas of the mushroom-shaped pillar on the paper and the line pattern substrate have a little difference, even though the overall tendency coincides with each other. This difference mainly resulted from the geometrical characteristics of the two substrates.

In the case of the paper substrate, there is no considerable change in contact area for Young's modulus from 500 MPa to 10 MPa, whereas the contact area sharply increases for the elastic modulus in the range of 10 to 0.01 MPa. In contrast, in the case of the line pattern substrate, the contact area changes throughout the whole range of Young's modulus. As a result, the contact area in the same Young's modulus is generally higher than the paper substrate because the universal shape of the line pattern substrate is flatter than the shape of the paper substrate.

Although there is a little difference in the graphs, the types of function for the approximation for the two cases are equivalent to the tendency of Young's modulus-contact area relations. The only different thing is the coefficients of functions while the types of functions are the power-law function. For the paper substrate, the constant of power law p_1 is relatively small and the absolute value of exponent p_2 is relatively large. For the line pattern substrate, the constant of power law l_1 is relatively large and the absolute value of exponent l_2 is relatively small.

3.3 Theoretical adhesion strengths

In the previous section, the contact areas according to the diverse Young's moduli were numerically predicted by the finite element method and the contact area-elastic modulus relations were defined for the paper and line pattern substrates. Subsequently in this chapter, the theoretical adhesion force of the mushroom-shaped pillar made of the e-PUA/PCL blend according to the change of Young's modulus and the contact area will be calculated and compared to the experimental adhesion force.

The theoretical adhesion force can be calculated by inserting the work of adhesion, Poisson's ratio, the radius of the pillar, elastic modulus and the numerically predicted contact area into equation 6. The values of work of adhesion obtained by equation 2 and table 2 (see chapter 3.5.1) are 81.2 mJ/m^2 and 42.66 mJ/m^2 for the paper and line-patterned substrates, respectively. Theoretical values of Poisson's ratio and radius of the pillar are clarified in chapter 3.5.1. As the measurement and calculation of the adhesion force assume that the e-PUA/PCL blend is in the modulus-recovered state after cooling for fixation, Young's modulus for the equation 6 is 210MPa (figure 12). The resulting theoretical adhesion strength with respect to Young's modulus for two different substrates are shown as graphs in figure 19.

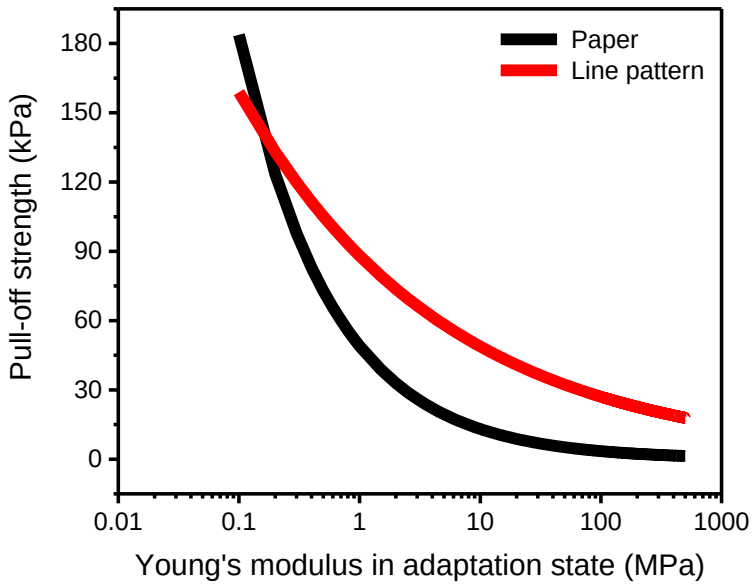

Figure 19 A graph describing the relation between theoretical adhesion strength versus Young's modulus of the e-PUA/PCL blend for the paper and line pattern substrates.

For both substrates, the relation showed a similar tendency with previously introduced relation between the contact area and Young's modulus (figure 16 and 18) because the pull-off strength of the

mushroom-shaped microstructure to the substrates is mainly determined by the contact area (equation 6 and figure 20).

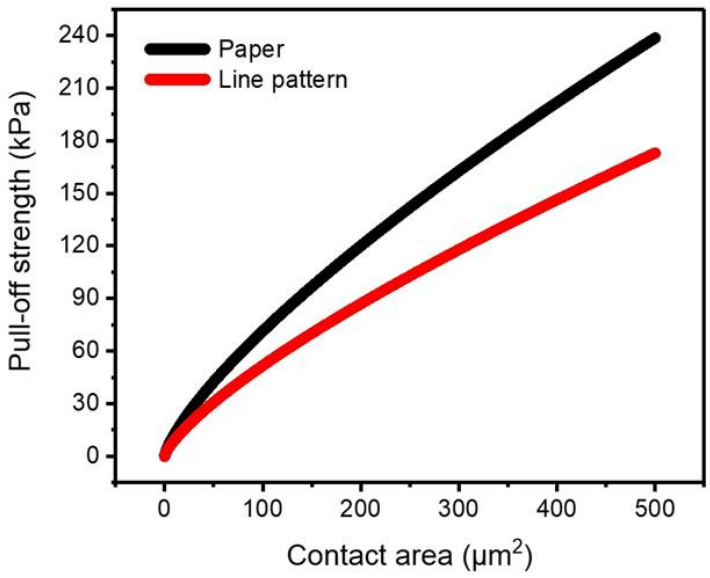

Figure 20 A graph describing the relation between theoretical adhesion strength versus the contact area for the paper and line pattern substrates, based on equation 6.

Based on these results, it is theoretically verified that the main components of adhesion enhancement mechanism utilizing shape-reconfigurable polymer are 1) the increased contact area due to the reduced elastic modulus in the adaptation process and 2) the recovered elastic modulus in fixation procedure.

3.4 Comparison of theoretical results with experimental measurements

The theoretical and experimental results of adhesion strengths of the mushroom-shaped pillar are compared, for both the paper and line pattern substrates in adapted and non-adapted states (figure 21 and 22). In the case of the paper substrate, the theoretical and experimental pull-off strengths of the non-adapted mushroom-shaped pillar are 2.257 kPa and 1.926 kPa, whereas those of adapted ones are 65.75 kPa and 71.05 kPa, respectively. For the line pattern substrate, the theoretical and experimental pull-off strengths of the non-adapted mushroom-shaped pillar are 22.26 kPa and 1.874 kPa, whereas those of adapted ones are 100.52 kPa and 124.73 kPa, respectively. The slight differences of adhesion strengths for the line pattern substrate result from the difference between the contact from FEA and mathematical approximation fitting. As the difference between the theoretical and experimental results is small, it is validated that the theoretical analysis of the adhesion enhancement mechanism in this research is reliable. It is proved that the shape-reconfigurable mushroom-shaped microstructure enhances the adhesion strength by the adaptation and the fixation processes with the aid of heat-responsive modulus tunability.

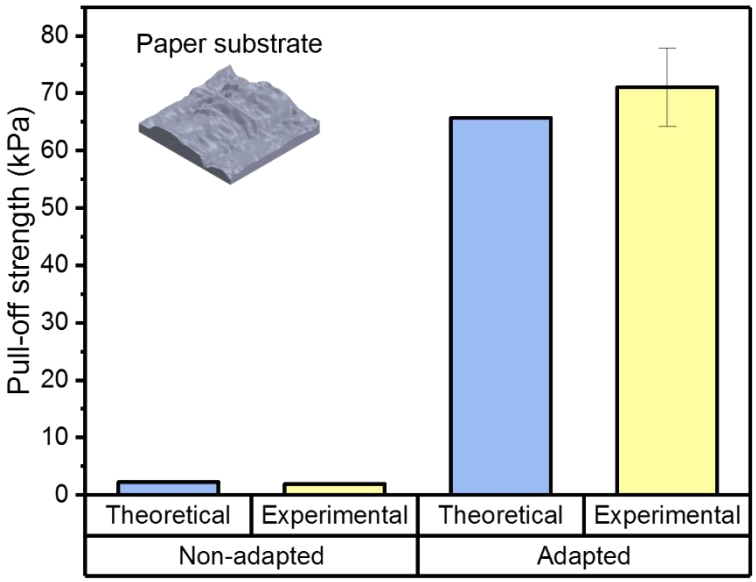

Figure 21 A graph describing the comparison between theoretical and experimental pull-off strength in adapted and non-adapted states for the paper substrate.

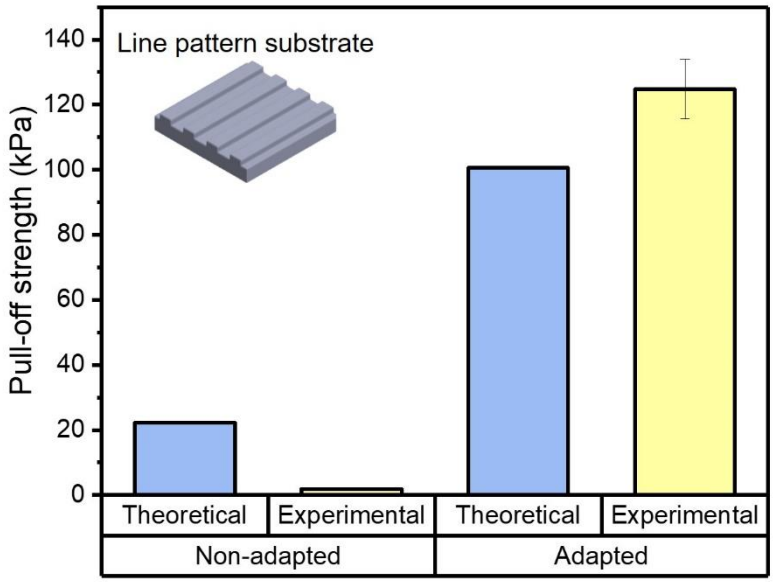

Figure 22 A graph describing the comparison between theoretical and experimental pull-off strength in adapted and non-adapted states for the line pattern substrate.

In summary, the contact areas of the mushroom-shaped pillar according to the variation in the elastic modulus on the predefined substrates were calculated by FEA. By the results, the relations between the contact area and Young's modulus were approximated the interaction formulas and graphs. Consequently, the relation between theoretical adhesion force and the elastic modulus was obtained by combining the JKR adhesion formula and FEA results. As stated in equation 6, the adhesion enhancement is mainly affected by Young's modulus and the contact area. As these physical quantities can be modulated actively using the e-PUA/PCL blend, the adhesion enhancement through the conformal adaptation with heat-stimulation and following fixation with cooling was confirmed theoretically. High accordance between the experimental measurement and numerical prediction of the adhesion strengths also implied strong reliability of this study.

3.5 Condition setup for numerical analysis

FEA was carried out for the calculation of the contact area of the mushroom-shaped pillar under mechanical loadings using general surface-to-surface contact interaction (Abaqus, Dassault Systèmes, France). The elastic and deformable microstructure models with different elastic moduli were modeled based on the theoretical values and experimentally-obtained mechanical properties. Detailed descriptions of material properties, modeling, boundary conditions, and mesh refinement are in the following sections.

3.5.1 Material properties

Based on the stress-strain curve in figure 12, the mushroom-shaped pillar was assumed as a linear elastic material. For the domain of the mushroom-shaped pillar, three material properties of the e-PUA/PCL blend, which are density, Young's modulus, and Poisson's ratio, were required for the numerical calculation. Young's moduli of the blend of e-PUA and PCL was set variously, which are 0.1 MPa, 1 MPa, 10 MPa, 100 MPa, and 500MPa. As the plastic deformation was not considered in this study, the properties related to plastic deformation such as yield stress or elongation at break were not considered. Poisson's ratio of the blend was set by referencing the value of existing studies presenting the Poisson's ratios of PUA and PCL respectively [51, 52]. The confirmed properties are listed in table 1.

Table 1. Material properties of the blend of e-PUA and PCL required for FEA.

Density	Young's modulus	Poisson's ratio
1100 kg/m^3	0.1, 1, 10, 100 and 500 MPa	0.45

For the domain of the substrates including the paper and line pattern, the dispersion and polar components of the surface energy of materials including the e-PUA/PCL blend, paper and PUA were properly given by literature [53-56]. The properties are listed in table 2.

Table 2. The dispersion and polar components of the surface energy of blend of e-PUA and PCL, paper and PUA.

	e-PUA+PCL	Paper	PUA
γ^d (mJ/m^2)	33.65	47.3	5.7
γ^p (mJ/m^2)	4.95	0.1	11.3

3.5.2 Substrate and mushroom-shaped pillar 3D modeling

As representative substrates with a few micro-scale rough surfaces, the paper substrate, and the line pattern substrate were designated in this study. Before calculating the contact area of the mushroom-shaped pillar, detailed modeling of substrates was conducted for following finite element analyses in Abaqus. As the paper has a random and complicated surface with micro-scaled wrinkles, the equipment named surface profiler that can measure surfaces of the paper was utilized for a reliable study. Three-dimensional data of the substrate were measured and exported using the surface profiler. The 3D-modeled substrate post-processed in Solidworks is presented in figure 23. As shown, the geometry of the paper substrate is highly complicated. The RMS of paper is about 18 μm. The line pattern substrate shown in figure 24 was directly modeled in Solidworks. The width, height, and fillet of the line pattern are 5 μm, 2 μm and 0.1 μm, respectively. The modeled substrates were then imported to Abaqus as the type of discrete rigid for subsequent finite element analyses.

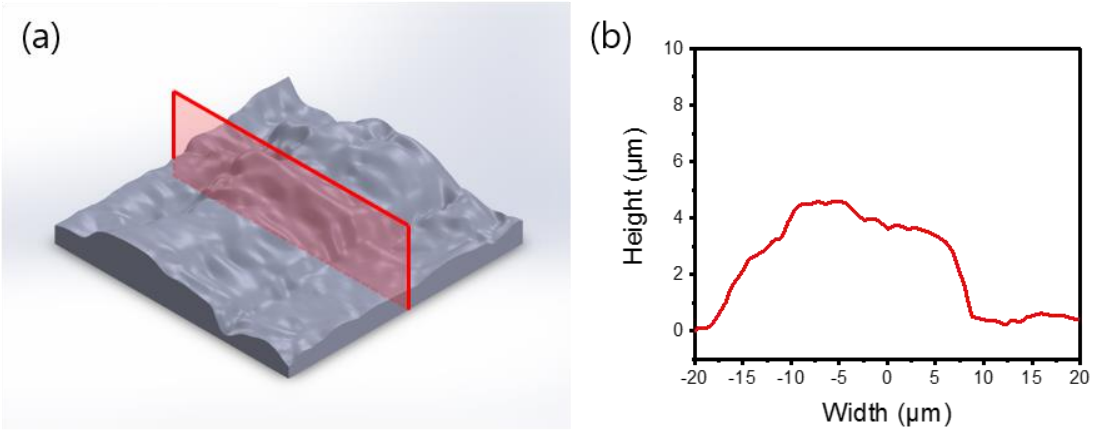

Figure 23 The paper substrate with micro-scale rough surfaces. (a) 3D model (b) cross-section line graph cut by the centerline of the substrate.

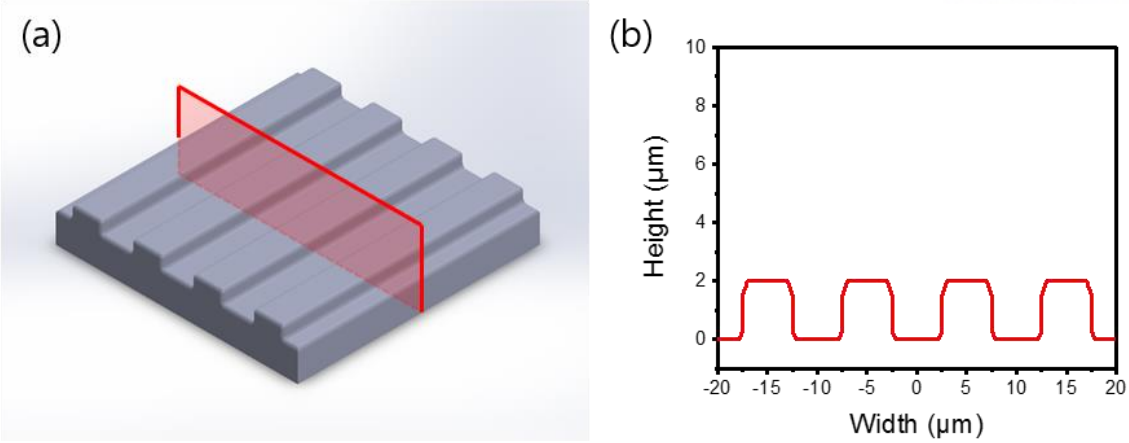

Figure 24 The line pattern substrate with micro-scale rough surfaces. (a) 3D model (b) cross-section line graph cut by the centerline of the substrate.

The mushroom-shaped pillar was modeled directly in Abaqus due to its simple geometry as shown in figure 25(a). Detailed dimensions of the mushroom-shaped pillar are presented in figure 25(b). The radius, height of the main pillar, width, thickness of tip, and fillet radius are 10 μm, 30 μm, 3 μm, 1 μm, and 0.5 μm, respectively.

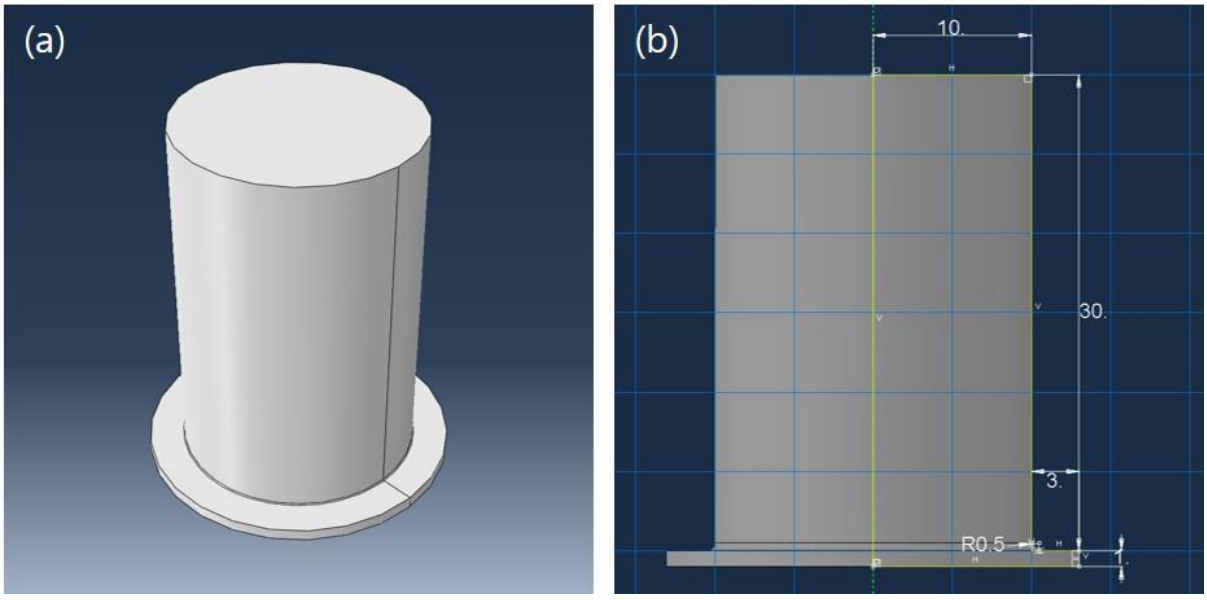

Figure 25 (a) 3D model of the mushroom-shaped pillar (b) geometrical dimension of mushroom-shaped pillar: radius of 10 μm, height of 30 μm, tip width of 3 μm, tip thickness of 1 μm, and fillet radius of 0.5 μm.

3.5.3 Boundary conditions

Boundary conditions of this FEA included the settlement of the substrate and the displacement of the mushroom-shaped pillar. The substrate settlement was conditioned by setting displacements in all directions to zero. Its boundary condition type in Abaqus is Symmetry/Antisymmetry/Encastre and the Encastre (U1 = U2 = U3 = UR1 = UR2 = UR3 = 0) was selected. The displacement of the mushroom-shaped pillar was conditioned by setting the displacement to zero in X and Z directions and to preset value in the Y direction. The boundary condition type of pillar upper part displacement was Displacement/Rotation. Two directions which are X and Z were set to 0 by checking U1 and U3 as 0 and the magnitude of movement in the Y direction was set differently at every case. The magnitudes of displacement in the Y direction were set so that the pressure pushing the microstructure down became 10 kPa for every case. Figure 26(a) and 26(b) describe that the boundary conditions were applied to paper and line pattern substrate, respectively.

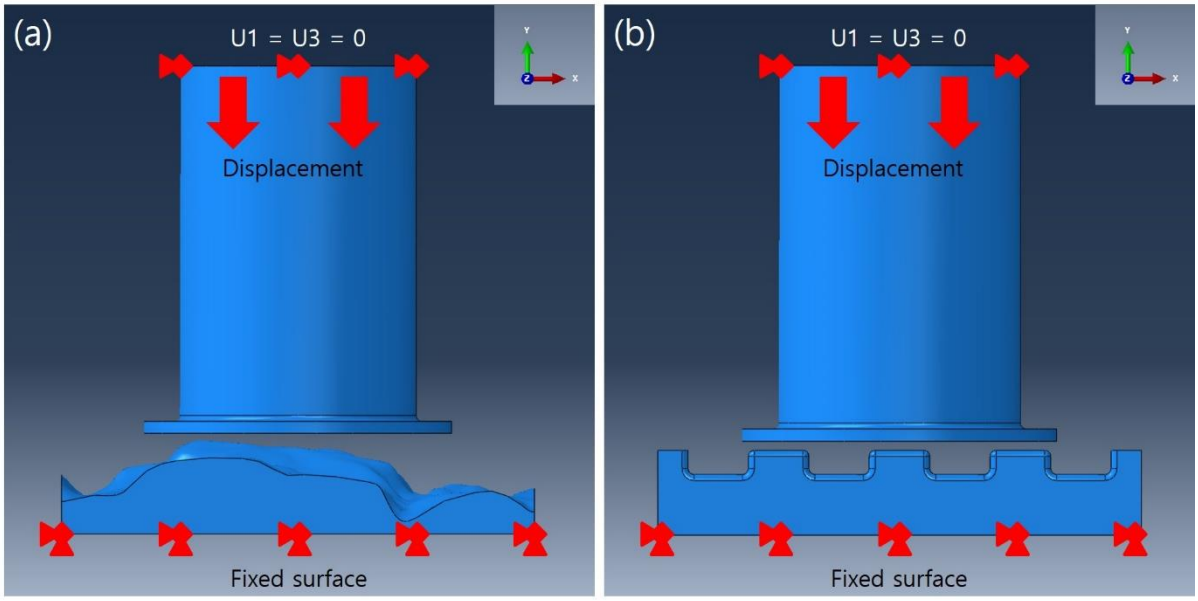

Figure 26 The boundary conditions of FEA analyzing the adhesion process. The mushroom-shaped pillar will approach to (a) the paper substrate (b) the line pattern substrate.

3.5.4 Mesh refinement

The mushroom-shaped pillar was designed to have hexahedral mesh in this study. The mesh size of the mushroom-shaped pillar is refined to be identical at every location excluding the fillet part for better convergence, as shown in Figure 27. The mesh size of the mushroom-shaped pillar except for the fillet part was determined to 0.5 μm, which was not too large or small value that leads to inaccurate calculation results or requirement for too many computing resources. The mesh size of the fillet part was determined to 0.25 μm for better convergence. The number of total nodes and elements of the mushroom-shaped pillar were 174580 and 165800, respectively.

The mesh size of the substrate was set variously according to the location in order to reduce the calculation time by refining only on the contacted part. The mesh size of the top part of the substrate directly contacting the mushroom-shaped pillar was determined to 1 μm which was a little larger than the mesh size of the mushroom-shaped pillar, whereas that of other parts was determined to 5 μm, as shown in figure 28 and 29. The number of total nodes and elements of the paper substrate was 2872 and 2870, respectively. The number of total nodes and elements of the line pattern substrate was 3861 and 3870, respectively. The arbitrary Lagrangian-Eulerian (ALE) adaptive mesh controls were also applied in this FEA because the deformation of the mushroom-shaped pillar was quite large.

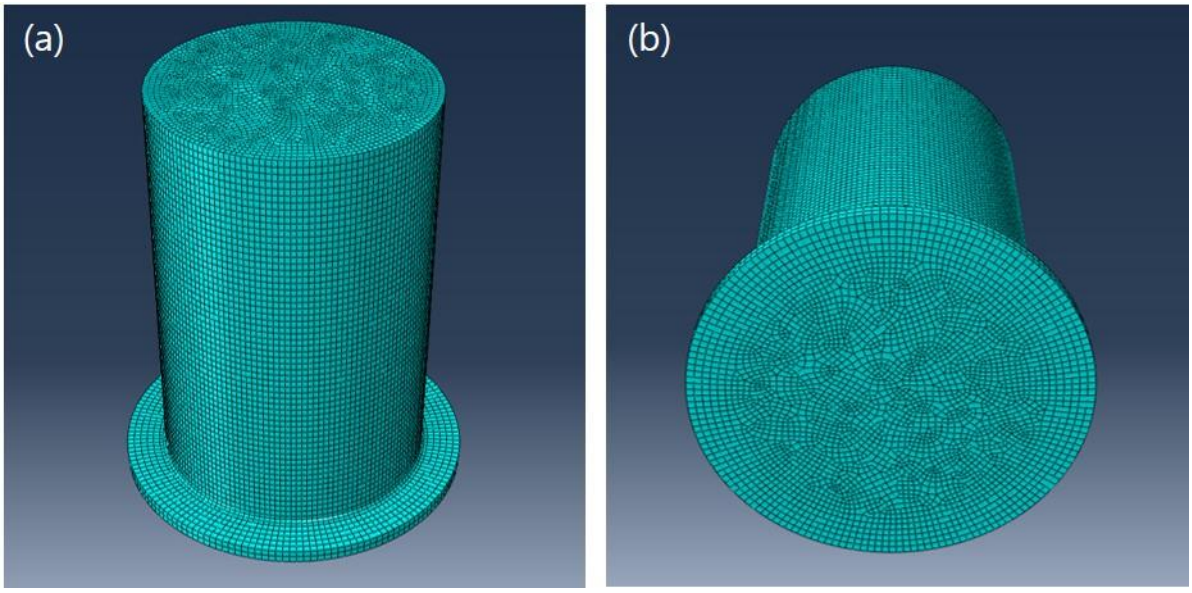

Figure 27 The meshed mushroom-shaped pillar having the size of mesh as 0.5 μm except for fillet part having the size of mesh as 0.25 μm. (a) upper view (b) lower view.

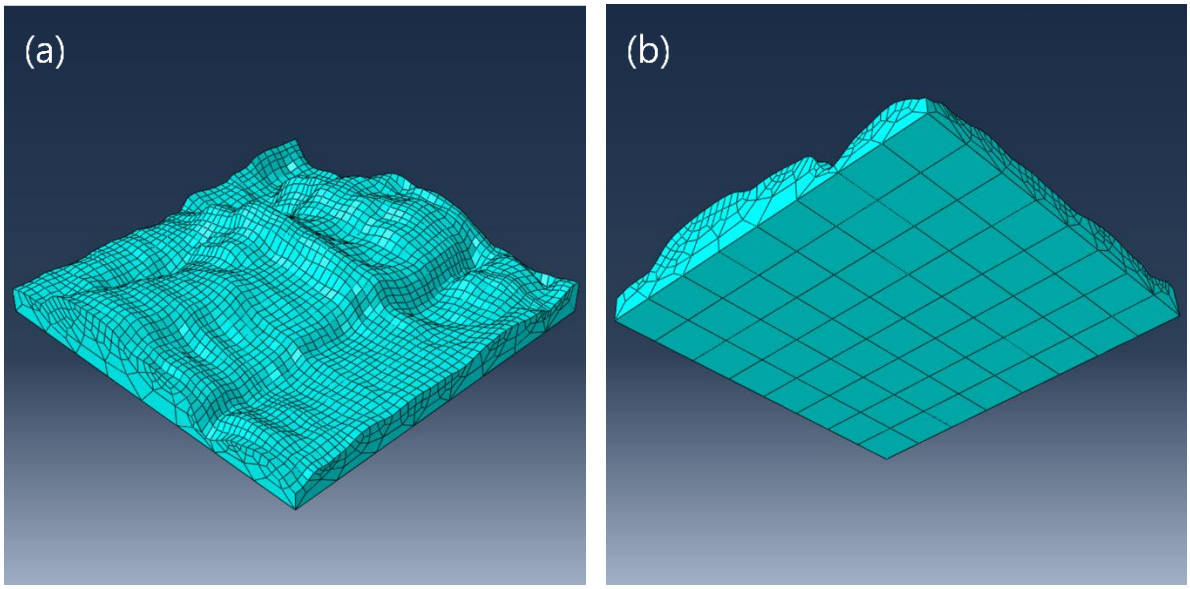

Figure 28 The meshed paper substrate having the size of mesh as 1 μm at the top area and 5 μm at other parts. (a) upper view (b) lower view.

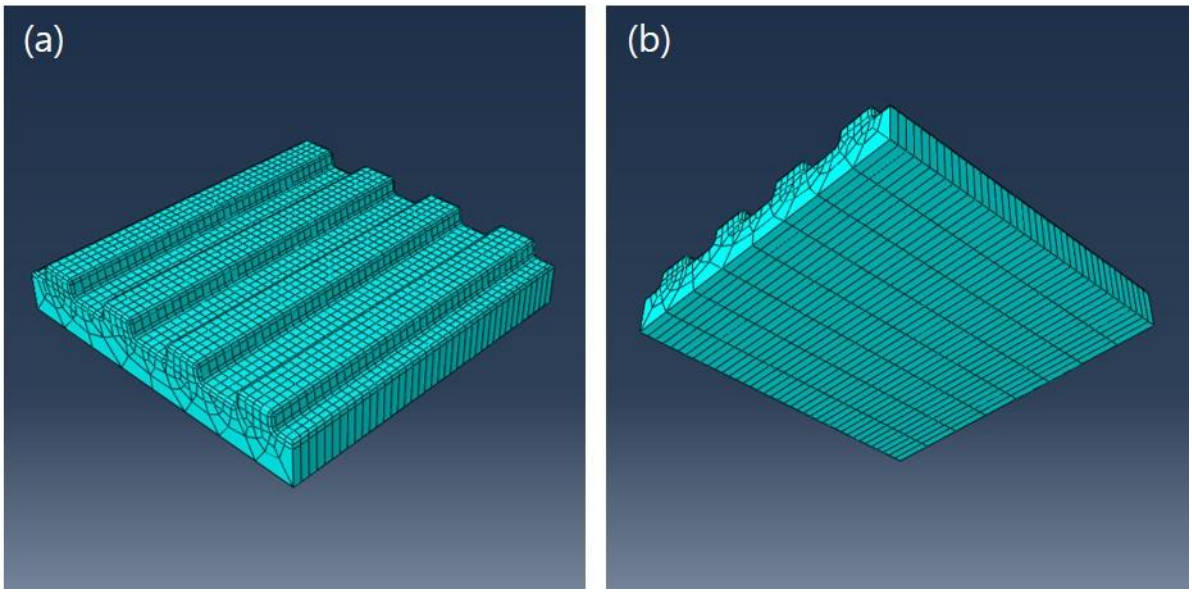

Figure 29 The meshed line pattern substrate having the size of mesh as 1 μm at the top area and 5 μm at other parts. (a) upper view (b) lower view.

The mesh quality was also checked using the built-in module. Figure 30 shows the mesh quality of parts. Since the mesh design of the substrates was quite simple, the warning marks highlighted by the yellow color existed only in the mushroom-shaped pillar. The yellow marks are not fatal issues but exhibit some low-quality elements. There were 2131 numbers of low-quality elements accounting for 1.285 % of total elements. All of them were in the fillet part.

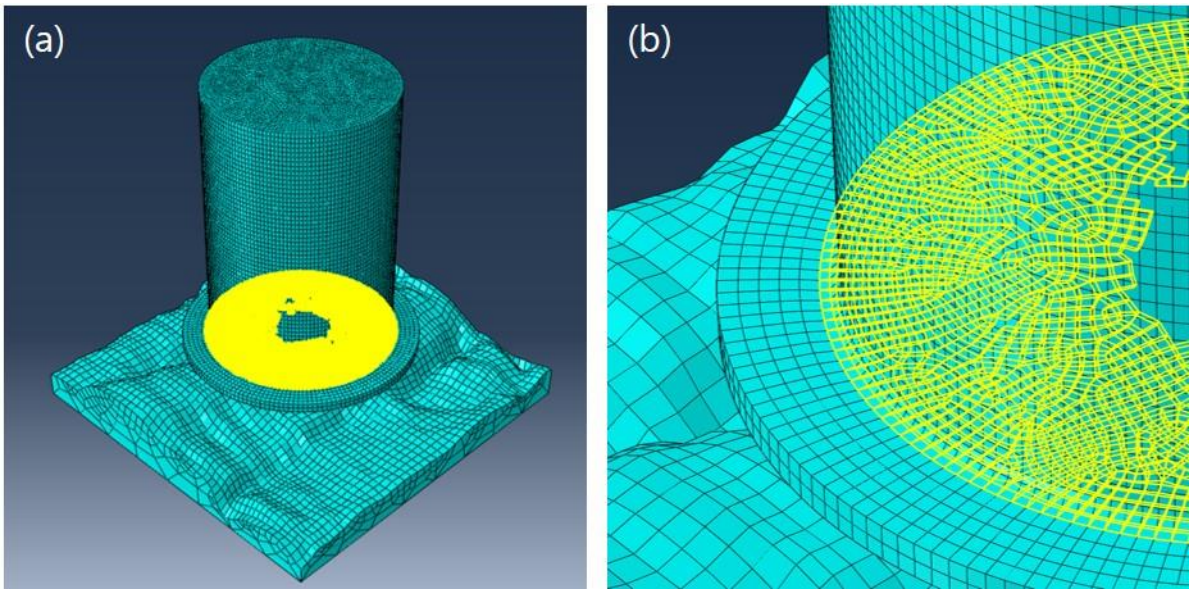

Figure 30 The picture after applying the Verify Mesh tool in Abaqus. There are some yellow marked low-quality elements. (a) whole view (b) zoom-in view.

4. Conclusion

In this thesis, we proposed the mushroom-shaped microstructure composed of a heat-responsive e-PUA/PCL blend that is highly adaptable onto rough surfaces with the aid of the elastic modulus-tunability. The adhesion enhancement mechanism was experimentally observed and theoretically analyzed.

In the experimental results (chapter 2), the adaptability of the mushroom-shaped pillar made of the blend of e-PUA and PCL to rough surfaces including the paper and line pattern substrates was observed and confirmed using microscopies. Heat-induced shape-reconfiguration, change in Young's modulus, and corresponding pull-off strength were also presented. The results indicated that the mushroom-shaped pillar array significantly enhances adhesion due to the enlarged contact area by surface-adaptation and fixation.

In the theoretical background (chapter 3), the formula of adhesion force was firstly obtained from the JKR model theory. The adhesion force formula from literature was modified into the appropriate form to use the contact area as a parameter. Further modification of the formula was conducted for unit consistency with the experimentally obtained values of adhesion strengths.

In the theoretical analysis (chapter 4), several preliminary setups were conducted to obtain correct results from the calculation in FEA. Firstly, the three-dimensional shapes of the mushroom-shaped pillar and two different substrates of paper and line patterns were modeled using a computer-aided design tool. Secondly, material properties such as density, the elastic modulus, and Poisson's ratio of the e-PUA/PCL blend were set. Especially, Young's moduli were set with various values of 0.1 MPa, 1 MPa, 10 MPa, 100 MPa, and 500 MPa to understand the relationship between the modulus and the contact area. Thirdly, boundary conditions including the position of the substrates and displacement of the mushroom-shaped pillar were established. Lastly, mesh refinement with proper shape and size for accurate and fast calculation was conducted. After all of these setup procedures, the structural deformation and corresponding change in contact area were numerically predicted. Consequently, the pull-off strength was calculated based on the previously built theoretical formula.

As a result, it was found out that the pull-off strength of the adapted mushroom-shaped pillar is much higher than the non-adapted one was because the adaptation process maximizes contact area both on the paper (> 88.45 times higher than the non-adapted state) and the line pattern substrate (> 7.41 times higher than non-adapted state). As the elastic modulus of the e-PUA/PCL blend is lowered to ~1 MPa by heating, the mushroom-shaped pillar became in a state of complete adaptation onto the surfaces of the paper and the line pattern substrates. Due to the subsequent recovery of the elastic modulus to ~200 MPa by cooling, the substrate-adapted mushroom-shaped pillar became in a state of fixation. In

conclusion, the adhesion enhancement mechanism has been investigated in this thesis by clarifying that adhesion of the mushroom-shaped pillar comprised of shape-reconfigurable polymer becomes stronger by two successive procedures, adaptation, and fixation. We believe that more versatile and smarter dry adhesives using stimuli-responsive material can be developed in the future through experimental and theoretical approaches and the result of the proposed study.

REFERENCES

[1] H. J. Gao, X. Wang, H. M. Yao, S. Gorb, and E. Arzt, "Mechanics of hierarchical adhesion structures of geckos," *Mech Mater,* vol. 37, no. 2-3, pp. 275-285, Feb-Mar 2005.

[2] A. K. Geim, S. V. Dubonos, I. V. Grigorieva, K. S. Novoselov, A. A. Zhukov, and S. Y. Shapoval, "Microfabricated adhesive mimicking gecko foot-hair," *Nat Mater,* vol. 2, no. 7, pp. 461-463, Jul 2003.

[3] K. Autumn *et al.*, "Adhesive force of a single gecko foot-hair," *Nature,* vol. 405, no. 6787, pp. 681-685, Jun 8 2000.

[4] W. X. Sun, P. Neuzil, T. S. Kustandi, S. Oh, and V. D. Samper, "The nature of the gecko lizard adhesive force," *Biophys J,* vol. 89, no. 2, pp. L14-L17, Aug 2005.

[5] Y. Tian *et al.*, "Adhesion and friction in gecko toe attachment and detachment," *P Natl Acad Sci USA,* vol. 103, no. 51, pp. 19320-19325, Dec 19 2006.

[6] J. M. R. Bullock and W. Federle, "Beetle adhesive hairs differ in stiffness and stickiness: in vivo adhesion measurements on individual setae," *Naturwissenschaften,* vol. 98, no. 5, pp. 381-387, May 2011.

[7] E. Gorb and S. Gorb, "Effects of surface topography and chemistry of Rumex obtusifolius leaves on the attachment of the beetle Gastrophysa viridula," *Entomol Exp Appl,* vol. 130, no. 3, pp. 222-228, Mar 2009.

[8] M. Varenberg, N. M. Pugno, and S. N. Gorb, "Spatulate structures in biological fibrillar adhesion," *Soft Matter,* vol. 6, no. 14, pp. 3269-3272, 2010.

[9] Y. M. Zhou, A. Robinson, U. Steiner, and W. Federle, "Insect adhesion on rough surfaces: analysis of adhesive contact of smooth and hairy pads on transparent microstructured substrates," *J R Soc Interface,* vol. 11, no. 98, Sep 6 2014.

[10] E. V. Gorb, N. Hosoda, C. Miksch, and S. N. Gorb, "Slippery pores: anti-adhesive effect of nanoporous substrates on the beetle attachment system," *J R Soc Interface,* vol. 7, no. 52, pp. 1571-1579, Nov 6 2010.

[11] K. Autumn *et al.*, "Evidence for van der Waals adhesion in gecko setae," *P Natl Acad Sci USA,* vol. 99, no. 19, pp. 12252-12256, Sep 17 2002.

[12] F. W. Delrio, M. P. De Boer, J. A. Knapp, E. D. Reedy, P. J. Clews, and M. L. Dunn, "The role of van der Waals forces in adhesion of micromachined surfaces," *Nat Mater,* vol. 4, no. 8, pp. 629-634, Aug 2005.

[13] S. N. Gorb and M. Varenberg, "Mushroom-shaped geometry of contact elements in biological adhesive systems," *J Adhes Sci Technol,* vol. 21, no. 12-13, pp. 1175-1183, Oct 2007.

[14] A. del Campo, C. Greiner, and E. Arzt, "Contact shape controls adhesion of bioinspired fibrillar surfaces," *Langmuir,* vol. 23, no. 20, pp. 10235-10243, Sep 25 2007.

[15] H. Yi *et al.*, "Bio-Inspired Adhesive Systems for Next-Generation Green Manufacturing," *Int J Pr Eng Man-Gt,* vol. 1, no. 4, pp. 347-351, Oct 2014.

[16] G. Carbone, E. Pierro, and S. N. Gorb, "Origin of the superior adhesive performance of mushroom-shaped microstructured surfaces," *Soft Matter,* vol. 7, no. 12, pp. 5545-5552, 2011.

[17] S. M. Kang, S. M. Kim, H. N. Kim, M. K. Kwak, D. H. Tahk, and K. Y. Suh, "Robust superomniphobic surfaces with mushroom-like micropillar arrays," *Soft Matter,* vol. 8, no. 33, pp. 8563-8568, 2012.

[18] M. Henrey, J. P. D. Tellez, K. Wormnes, L. Pambaguian, and C. Menon, "Towards the use of mushroom-capped dry adhesives in outer space: Effects of low pressure and temperature on adhesion strength," *Aerosp Sci Technol,* vol. 29, no. 1, pp. 185-190, Aug 2013.

[19] D. Sameoto, H. Sharif, and C. Menon, "Investigation of low-pressure adhesion performance of mushroom shaped biomimetic dry adhesives," *J Adhes Sci Technol,* vol. 26, no. 23, pp. 2641-2652, 2012.

[20] D. Sameoto and C. Menon, "A low-cost, high-yield fabrication method for producing optimized biomimetic dry adhesives," *J Micromech Microeng,* vol. 19, no. 11, Nov 2009.

[21] C. K. Hossfeld, A. S. Schneider, E. Arzt, and C. P. Frick, "Detachment Behavior of Mushroom-Shaped Fibrillar Adhesive Surfaces in Peel Testing," *Langmuir,* vol. 29, no. 49, pp. 15394-15404, Dec 10 2013.

[22] C. Luo, F. Meng, and A. Francis, "Fabrication and application of silicon-reinforced PDMS masters," *Microelectron J,* vol. 37, no. 10, pp. 1036-1046, Oct 2006.

[23] K. Shah, W. C. Shin, and R. S. Besser, "A PDMS micro proton exchange membrane fuel cell by conventional and non-conventional microfabrication techniques," *Sensor Actuat B-Chem,* vol. 97, no. 2-3, pp. 157-167, Feb 1 2004.

[24] H. L. Cong and T. R. Pan, "Photopatternable conductive PDMS materials for microfabrication," *Adv Funct Mater,* vol. 18, no. 13, pp. 1912-1921, Jul 9 2008.

[25] R. W. R. L. Gajasinghe *et al.*, "Experimental study of PDMS bonding to various substrates for monolithic microfluidic applications," *J Micromech Microeng,* vol. 24, no. 7, Jul 2014.

[26] S. J. Hwang *et al.*, "Dry etching of polydimethylsiloxane using microwave plasma," *J Micromech Microeng,* vol. 19, no. 9, Sep 2009.

[27] H. Yi, M. Kang, M. K. Kwak, and H. E. Jeong, "Simple and Reliable Fabrication of Bioinspired Mushroom-Shaped Micropillars with Precisely Controlled Tip Geometries," *Acs Appl Mater Inter,* vol. 8, no. 34, pp. 22671-22678, Aug 31 2016.

[28] H. Kasem and M. Varenberg, "Effect of counterface roughness on adhesion of mushroom-shaped microstructure," *J R Soc Interface,* vol. 10, no. 87, Oct 6 2013.

[29] D. M. Drotlef, M. Amjadi, M. Yunusa, and M. Sitti, "Bioinspired Composite Microfibers for Skin Adhesion and Signal Amplification of Wearable Sensors," *Adv Mater,* vol. 29, no. 28, Jul 26 2017.

[30] M. K. Kwak, H. E. Jeong, and K. Y. Suh, "Rational Design and Enhanced Biocompatibility of a Dry Adhesive Medical Skin Patch," *Adv Mater,* vol. 23, no. 34, pp. 3949-+, Sep 8 2011.

[31] H. Wang, G. Pastorin, and C. Lee, "Toward Self-Powered Wearable Adhesive Skin Patch with Bendable Microneedle Array for Transdermal Drug Delivery," *Adv Sci,* vol. 3, no. 9, Sep 2016.

[32] I. Hwang *et al.*, "Multifunctional Smart Skin Adhesive Patches for Advanced Health Care," *Adv Healthc Mater,* vol. 7, no. 15, Aug 8 2018.

[33] H. Yi *et al.*, "Ultra-Adaptable and Wearable Photonic Skin Based on a Shape-Memory, Responsive Cellulose Derivative," *Adv Funct Mater,* vol. 29, no. 34, Aug 2019.

[34] M. Seong, J. Lee, I. Hwang, and H. E. Jeong, "Significant Adhesion Enhancement of Bioinspired Dry Adhesives by Simple Thermal Treatment," *Int J Pr Eng Man-Gt,* vol. 6, no. 3, pp. 587-599, Jul 2019.

[35] T. Kim, J. Park, J. Sohn, D. Cho, and S. Jeon, "Bioinspired, Highly Stretchable, and Conductive Dry Adhesives Based on 1D-2D Hybrid Carbon Nanocomposites for All-in-One ECG Electrodes," *Acs Nano,* vol. 10, no. 4, pp. 4770-4778, Apr 2016.

[36] G. Castellanos, E. Arzt, and M. Kamperman, "Effect of Viscoelasticity on Adhesion of Bioinspired Micropatterned Epoxy Surfaces," *Langmuir,* vol. 27, no. 12, pp. 7752-7759, Jun 21 2011.

[37] C. Liu, H. Qin, and P. T. Mather, "Review of progress in shape-memory polymers," *J Mater Chem,* vol. 17, no. 16, pp. 1543-1558, 2007.

[38] H. Z. Wu, P. Chen, C. Z. Yan, C. Cai, and Y. S. Shi, "Four-dimensional printing of a novel acrylate-based shape memory polymer using digital light processing," *Mater Design,* vol. 171, Jun 5 2019.

[39] Y. Zhu *et al.*, "Rapidly switchable water-sensitive shape-memory cellulose/elastomer nano-composites," *Soft Matter,* vol. 8, no. 8, pp. 2509-2517, 2012.

[40] W. Feng, W. F. Zhou, S. D. Zhang, Y. J. Fan, A. Yasin, and H. Y. Yang, "UV-controlled shape memory hydrogels triggered by photoacid generator," *Rsc Adv,* vol. 5, no. 100, pp. 81784-81789, 2015.

[41] K. P. Mineart, S. S. Tallury, T. Li, B. Lee, and R. J. Spontak, "Phase-Change Thermoplastic Elastomer Blends for Tunable Shape Memory by Physical Design," *Ind Eng Chem Res,* vol. 55, no. 49, pp. 12590-12597, Dec 14 2016.

[42] H. Meng, J. Zheng, X. F. Wen, Z. Q. Cai, J. W. Zhang, and T. Chen, "pH- and Sugar-Induced Shape Memory Hydrogel Based on Reversible Phenylboronic Acid-Diol Ester Bonds," *Macromol Rapid Comm,* vol. 36, no. 6, pp. 533-537, Mar 2015.

[43] H. Zhang, H. T. Wang, W. Zhong, and Q. G. Du, "A novel type of shape memory polymer blend and the shape memory mechanism," *Polymer,* vol. 50, no. 6, pp. 1596-1601, Mar 6 2009.

[44] Y. D. Wang, G. A. Ameer, B. J. Sheppard, and R. Langer, "A tough biodegradable elastomer," *Nat Biotechnol,* vol. 20, no. 6, pp. 602-606, Jun 2002.

[45] R. Pelrine, R. Kornbluh, J. Joseph, R. Heydt, Q. B. Pei, and S. Chiba, "High-field deformation of elastomeric dielectrics for actuators," *Mat Sci Eng C-Bio S,* vol. 11, no. 2, pp. 89-100, Nov 2000.

[46] Y. J. Chen, J. Sun, Y. J. Liu, and J. S. Leng, "Variable stiffness property study on shape memory polymer composite tube," *Smart Mater Struct,* vol. 21, no. 9, Sep 2012.

[47] V. Vaenkatesan, Z. L. Li, W. P. Vellinga, and W. H. de Jeu, "Adhesion and friction behaviours of polydimethylsiloxane - A fresh perspective on JKR measurements," *Polymer,* vol. 47, no. 25, pp. 8317-8325, Nov 22 2006.

[48] K. L. Johnson and I. Sridhar, "Adhesion between a spherical indenter and an elastic solid with a compliant elastic coating," *J Phys D Appl Phys,* vol. 34, no. 5, pp. 683-689, Mar 7 2001.

[49] H. Cho *et al.*, "Intrinsically reversible superglues via shape adaptation inspired by snail epiphragm," *P Natl Acad Sci USA,* vol. 116, no. 28, pp. 13774-13779, Jul 9 2019.

[50] W. C. Hamilton, "Measurement of Polar Force Contribution to Adhesive Bonding," *J Colloid Interf Sci,* vol. 47, no. 3, pp. 672-675, 1974.

[51] H. J. Qi and M. C. Boyce, "Stress-strain behavior of thermoplastic polyurethanes," *Mech Mater,* vol. 37, no. 8, pp. 817-839, Aug 2005.

[52] L. Lu *et al.*, "Mechanical study of polycaprolactone-hydroxyapatite porous scaffolds created by porogen-based solid freeform fabrication method," *J Appl Biomater Func,* vol. 12, no. 3, pp. 145-154, 2014.

[53] H. Yi *et al.*, "Continuous and Scalable Fabrication of Bioinspired Dry Adhesives via a Roll-to-Roll Process with Modulated Ultraviolet-Curable Resin," *Acs Appl Mater Inter,* vol. 6, no. 16, pp. 14590-14599, Aug 27 2014.

[54] L. C. Lins, V. Bugatti, S. Livi, and G. Gorrasi, "Ionic Liquid as Surfactant Agent of Hydrotalcite: Influence on the Final Properties of Polycaprolactone Matrix," *Polymers-Basel,* vol. 10, no. 1, Jan 2018.

[55] M. S. Saraiva, J. A. F. Gamelas, A. P. M. de Sousa, B. M. Reis, J. L. Amaral, and P. J. Ferreira, "A New Approach for the Modification of Paper Surface Properties Using Polyoxometalates," *Materials,* vol. 3, no. 1, pp. 201-215, Jan 2010.

[56] J. K. Kim *et al.*, "Effect of surface tension and coefficient of thermal expansion in 30 nm scale nanoimprinting with two flexible polymer molds," *Nanotechnology,* vol. 23, no. 23, Jun 15 2012.